Research Square

Preprints are preliminary reports that have not undergone peer review.
They should not be considered conclusive, used to inform clinical practice,
or referenced by the media as validated information.

Global phylogeography of H10Nx avian influenza reveals regional persistence and an intensifying poultry-associated spillover interface

Dongchang He
Jiangsu Agri-Animal Husbandry Vocational College
Ting Wang
Jiangsu Agri-Animal Husbandry Vocational College
Min Gu
Yangzhou University
Yongjuan Wang
tzuvet@outlook.com

Jiangsu Agri-Animal Husbandry Vocational College

Research Article

Keywords: H10Nx avian influenza virus, phylogeography, trunk persistence, host transition, zoonotic spillover

Posted Date: June 25th, 2026

DOI: https://doi.org/10.21203/rs.3.rs-9965973/v1

License: This work is licensed under a Creative Commons Attribution 4.0 International License.
Read Full License

Additional Declarations: No competing interests reported.

Global phylogeography of H10Nx avian influenza reveals regional persistence and an intensifying poultry-associated spillover interface

Dongchang He [1,2], Ting Wang[1], Min Gu[2,3], Yongjuan Wang[1]

[1] School of Veterinary Medicine and Public Health, Jiangsu Agri-Animal Husbandry Vocational College, Taizhou 225300, China.

[2]Jiangsu Key Laboratory of Zoonosis, Yangzhou University, Yangzhou, 225009, China.

[3]Animal Infectious Disease Laboratory, College of Veterinary Medicine, Yangzhou University; Yangzhou, Jiangsu 225009, China

*** Correspondence:** Yongjuan Wang, tzuvet@outlook.com

Abstract

Influenza A viruses are maintained primarily in wild aquatic birds, but H10Nx viruses have repeatedly crossed host barriers into poultry, mammals, and humans. Despite increasing reports of reassortment, host expansion, and sporadic human infection, the global circulation history of H10Nx remains poorly resolved. Here, we assembled 1,045 non-redundant global H10Nx virus sequences collected from 1949 to 2023 and analyzed a clock-filtered dataset of 824 HA sequences using time-scaled phylogenetics, Bayesian phylogeography, source-sink inference, trunk persistence analysis, and site-level evolutionary screening. We found that H10Nx evolution is dominated by regionally structured persistence within major transmission pools, especially Atlantic America, East Asia, and Europe, rather than by frequent sustained intercontinental mixing. Anas-associated lineages contributed disproportionately to the long-term evolutionary backbone, whereas host-transition analyses supported a stepwise diffusion pattern from ducks to chickens and then sporadically to mammals. Within China, phylogeographic reconstruction revealed a sequential shift from an early Hong Kong-Hubei-Jiangxi focus to a Jiangxi-centered dissemination network and, more recently, to the eastern coastal provinces, especially Jiangsu, Shanghai, and Zhejiang. Parallel evolution analysis identified recurrent substitutions at HA residue 130 as a candidate adaptive signal associated with recent host expansion. Overall, H10Nx follows a structured metapopulation model in which duck-associated maintenance, poultry amplification, and episodic long-distance lineage seeding jointly shape global diversification. These findings provide a clearer evolutionary framework for interpreting the continued emergence of H10Nx viruses at the duck-chicken-human interface.

Keywords: H10Nx avian influenza virus; phylogeography; trunk persistence; host transition; zoonotic

spillover

Introduction

Influenza A viruses are maintained primarily in wild aquatic birds, particularly members of the orders Anseriformes and Charadriiformes, which constitute the major natural reservoir of avian influenza diversity [1, 2]. The H10 subtype was first isolated from chickens in Germany in 1949 and has since been detected in both wild birds and domestic poultry worldwide [2–4]. Although H10 viruses are generally classified as low-pathogenic avian influenza viruses in birds, repeated detections in mammals and humans have raised sustained concern about their zoonotic potential [4]. They have attracted increasing attention because their host range is broader than previously assumed [2, 4]. Cross-species infection has been documented in mink, swine, harbor seals, and humans, including human infections with H10N7, H10N8, H10N3, and, more recently, H10N5 [2, 5–7]. These observations indicate that H10Nx viruses can repeatedly cross host barriers even when they circulate inconspicuously in avian populations.

In China, H10 viruses have attracted particular attention because long-term surveillance has shown movement from migratory birds into domestic ducks and then into live-poultry markets, where reassortment with enzootic H9N2 viruses contributed to the emergence of human-linked H10N8 and poultry H10N6 viruses [2]. Subsequent studies on H10N3 and H10N5 further suggested that the wild bird-poultry interface continues to provide opportunities for reassortment and sporadic spillover [8, 9]. At the same time, recent work has shown that the global H10 gene pool is structured into Eurasian and North American lineages, but this structure is increasingly blurred by intercontinental gene flow and recurrent reassortment [1, 2, 10, 11]. North American-origin H10 genes have now been detected in East Asian wild birds, and some of these viruses are phylogenetically linked to lineages associated with recent human H10N5 emergence [1, 10–12].

The long-term global circulation history of H10Nx remains incompletely resolved [1, 2, 10, 11]. Most available studies focus on specific outbreaks, host species, or regional surveillance windows, limiting inference on how regional persistence, long-distance dispersal, and host transitions interact over decades [2, 9–11]. It remains unclear whether global H10Nx dissemination reflects frequent panmictic intercontinental mixing or a structured metapopulation maintained by regional persistence and episodic long-distance seeding [10]. While the role of wild birds is widely acknowledged, the specific host groups and geographic regions that disproportionately sustain the viral evolutionary backbone (trunk ancestry) remain unquantified. Resolving these dynamics requires a unified analytical approach that integrates discrete transition modeling with continuous spatial diffusion and explicit host-state reconstruction [13].

In this study, we assembled a comprehensive dataset of 1,045 global H10Nx sequences sampled from 1949 to 2023 to reconstruct the evolutionary history, geographic diffusion, and host-transition dynamics

of the virus. By integrating discrete Bayesian phylogeography, jump-and-reward source-sink analysis, continuous relaxed-random-walk (RRW) modeling, and trunk persistence (PACT) analysis, we characterize the spatiotemporal architecture of global and China-specific H10Nx spread. We further assess the evolutionary pressures shaping recent host expansion by identifying parallel amino acid substitutions and evaluating receptor-binding energetics. Our analyses delineate the major geographic and host reservoirs that seed regional outbreaks and clarify the mechanisms underlying the repeated emergence of H10 lineages at the duck-chicken-human interface.

Methods

1. Data Collection and Sequence Cleaning

Whole-genome sequences and metadata of all globally reported H10Nx avian influenza viruses were retrieved from the GISAID EpiFlu™ database (https://www.gisaid.org) in January 2023. Sequences were filtered sequentially by [14]: (1) removing incomplete sequences (<90% ORF completeness); (2) excluding records with missing or ambiguous host or geographic information; (3) discarding records with incomplete or erroneous collection dates. Identical sequences were then removed using BioAider (v1.423) at a 100% identity threshold [15], yielding 1,045 non-redundant H10Nx sequences for downstream analyses.

2. Metadata Standardization

To satisfy the decimal-date requirements of BEAST, collection dates with missing month were imputed as June 15 of the corresponding year (YYYY-06-15), and those with month but missing day were imputed as the 15th of that month (YYYY-MM-15), following established practice in our previous studies [14, 16] Strains were assigned to four temporal strata by isolation year: 1949–1990, 1991–2000, 2001–2010, and 2011–2023, reflecting shifts in sampling intensity and global surveillance capacity across these periods. Host metadata were parsed into a standardized taxonomic hierarchy using custom R (v4.0.5) scripts: each strain's host name was resolved to its lowest identifiable taxonomic unit, higher-level ranks were supplemented via the NCBI Taxonomy database, and unresolvable entries were recorded as "Unknown." Geographic metadata were standardized to a three-tier hierarchy (country → province/state → city/county); textual location strings were converted to coordinates using the Local Focus Geocoding Service (https://geocode.localfocus.nl/), and non-standard or missing entries were corrected accordingly to support downstream spatiotemporal analyses.

3. Spatiotemporal Epidemiological Visualization

To characterize the epidemiological structure and multidimensional metadata associations of H10Nx avian influenza viruses, Sankey diagrams were constructed to visualize relationships among viral

subtype (H10N1, H10N2, H10N3, etc.), host taxonomy (at the Class or Order/Family level), isolation period, and continent of isolation (Asia, Europe, North America, South America, Oceania, Africa). Metadata aggregation was performed using the tidyverse suite. Diagrams were rendered within the ggplot2 (v3.3.5) framework using the ggsankey package (https://github.com/davidsjoberg/ggsankey); node widths were scaled proportionally to strain counts and flow colors encoded by subtype or period to reflect association strengths across biological and spatiotemporal attributes.

For the final temporally filtered world dataset (n = 824; see Section 5 for filtering details), collection localities were resolved to province- or state-level administrative units and geocoded to centroid coordinates using the R package tidygeocoder. K-means clustering was applied to latitude/longitude pairs (stats::kmeans, k = 8, iter.max = 10, nstart = 5). Two clusters were subsequently excluded: the Iceland cluster (n = 3; EPIISL379991–EPIISL379992), whose sequence density was disproportionately inflated relative to geographic area due to concentrated historical surveillance rather than true population structure, and the Oceania cluster (n = 1), which was too small to support reliable ancestral-state reconstruction in BEAST. The remaining six regions were retained for discrete phylogeographic analysis: Africa (n = 21), Europe (n = 94), East Asia (n = 166), Northeast Asia (n = 43), Atlantic America (n = 388), and Pacific America (n = 109).

4. Maximum Likelihood Phylogenetic Analysis

Maximum likelihood (ML) phylogenetic trees were constructed independently for all eight gene segments (PB2, PB1, PA, HA, NP, NA, M, NS) within the PhyloSuite (v1.2.2) using IQ-TREE [17, 18]. Sequences for each segment were aligned with MAFFT (v7.453) and manually trimmed to complete coding regions. The optimal substitution model was selected by ModelFinder [19] under the Bayesian Information Criterion (BIC). Node support was evaluated with 1,000 bootstrap replicates. All trees were rooted at the midpoint and visualized with ggtree and ggtreeExtra [20, 21].

5. Temporal Signal Detection and Dataset Subsampling

Among the 1,045 non-redundant records, only HA sequences with complete metadata were retained for temporal analysis, after which molecular clock outliers were removed by TreeTime (v0.8.1) [22] via root-to-tip regression against sampling dates. Sequences whose residuals exceeded four interquartile ranges (IQR) from the regression line were flagged as molecular clock outliers and excluded under the default --clock-filter criterion. The coefficient of determination (R^2) of the retained dataset was calculated to confirm adequate clock signal for downstream Bayesian analysis. Strains from China were extracted from this dataset to form an independent China (CN) dataset for targeted within-country phylogeographic inference.

6. Discrete Bayesian Phylogeographic Analysis

Discrete Bayesian phylogeographic analysis was conducted in BEAST (v1.10.4). The XML files were configured in BEAUti specifying a GTR+G4 nucleotide substitution model, an uncorrelated lognormal relaxed molecular clock, and a Bayesian SkyGrid coalescent tree prior (50 grid points; cutoff set to span the root age of each dataset) [23]. To reconstruct spatial diffusion, we employed an asymmetric continuous-time Markov chain (CTMC) model with Bayesian stochastic search variable selection (BSSVS) to identify statistically supported migration pathways; support was evaluated using Bayes factors and posterior probabilities. Markov jump and reward counts were simultaneously estimated to quantify specific state-to-state transition frequencies and to assess the relative contribution (source-sink structure) of each geographic region and host group.

MCMC chains were run for 2×10^8 generations, with sampling every 20,000 steps; the initial 10% of the trajectories were discarded as burn-in. Chain convergence was assessed using Tracer (v1.7), confirming that all parameters reached an effective sample size (ESS) > 200. Maximum clade credibility (MCC) trees were generated from the posterior tree distribution using TreeAnnotator. Migration events and state rewards were then quantified by parsing the posterior MCC trees using the migration-counting framework of Vargas et al. [24]. For the CN dataset, the same framework—implemented via the ETE Toolkit (v3.1.1)—traversed the time-scaled MCC tree in 1-year sliding windows to enumerate province-to-province and host-level migration branches annually, fully resolving the within-China transmission network.

7. Continuous Phylogeographic Reconstruction

Continuous phylogeographic analyses were performed separately for the world and CN datasets in BEAST (v1.10.4) under a Cauchy relaxed random walk (RRW) framework, following the protocol of Dellicour et al. [25]. For each dataset, BEAUti was used to add a bivariate continuous trait (latitude, longitude) to the sequence partition; ancestral location states were estimated at all internal nodes, and spatial diffusion was modeled along the time-scaled phylogeny using the Cauchy RRW process. A small random jitter (window = 0.01 decimal degrees) was applied to duplicated sampling coordinates to stabilize numerical performance. Country-level centroid coordinates were assigned to world-dataset strains to capture intercontinental spread; province-level centroids were assigned to CN-dataset strains to resolve within-China dispersal. MCMC settings and MCC tree summarization followed above section. Annotated MCC trees and posterior tree distributions were analyzed in R (v4.0.5) using the seraphim package (https://github.com/sdellicour/seraphim) to map lineage dispersal trajectories through time and compute branch-specific dispersal statistics [26, 27].

8. PACT-Based Host and Geographic Transition Dynamics

Time-varying migration dynamics and long-term trunk persistence were quantified by analyzing the full

posterior tree distributions from the discrete-trait BEAST runs using PACT (Posterior Analysis of Coalescent Trees; https://github.com/trvrb/PACT) . Unlike single MCC tree summaries, PACT integrates phylogenetic uncertainty across the entire posterior sample to estimate lineage counts, inter-state transition rates, and the proportion of trunk ancestry (the evolutionary backbone of the phylogeny) with robust credible intervals. For the CN dataset, posterior trees annotated by Chinese province and host genus (*Anas, Arenaria, Fulica, Gallus, Homo, Sus,* and others) or environmental source were analyzed separately to reconstruct province-to-province and host-genus transition events over time. For the world dataset, posterior trees annotated by the six geographic regions and host genus or environmental source were processed in parallel to estimate intercontinental and inter-host migration intensities. Both runs produced skyline trajectories of time-varying lineage counts and transition rates, together with overall transition frequency summaries, characterizing the spatiotemporal spread and host-switching dynamics of H10Nx viruses.

9. Episodic Selection and Parallel Evolution Analyses

Site-specific episodic diversifying selection in the HA gene was tested with the Mixed Effects Model of Evolution (MEME) [28] & Fast Unconstrained Bayesian AppRoximation (FUBAR)[29] in HyPhy (v2.5.31), applied to the 824-sequence global dataset HA alignment. MEME detects transient positive selection at individual codon sites across a subset of branches using a likelihood-ratio framework under default settings. Branch-wise amino acid substitution patterns were mapped onto the HA phylogeny using TreeSub (https://github.com/tamuri/treesub), which internally invokes RAxML to construct a maximum likelihood tree, reconstructs ancestral sequences, and annotates each branch with nonsynonymous changes. The resulting substitution-annotated tree was parsed and visualized in R (v4.0.5) with treeio [30] and ggtree [21]. Phylogeny-based sequence clustering was performed with the R/Bioconductor package sitePath (v1.26.0) [31], using the HA MCC tree from above as input. SitePath [31] jointly considers polymorphic sites and their phylogenetic adjacency to derive mutation-pattern groupings consistent with the underlying tree topology.

10. Molecular Dynamics Simulation and Receptor Binding Energetics

To assess how positively selected receptor-binding site (RBS) mutations alter sialic acid (SIA) binding, we performed explicit-solvent molecular dynamics simulations and end-state free energy calculations in Amber 20 [32]. The H10N8 HA co-crystal structures with an avian α2,3-linked receptor analog (3-SLN, PDB: 5TGV, https://www.rcsb.org/structure/5TGV) and a human α2,6-linked receptor analog (6-SLN, PDB: 5TH1, https://www.rcsb.org/structure/5TH1) were used as wild-type templates [33], and point mutations (K145Q and Q220R) were introduced in silico using UCSF Chimera v1.14. Ligands were parameterized with GAFF and AM1-BCC charges generated by Antechamber, proteins with the ff14SB force field, and each HA–SIA complex was prepared in tleap, neutralized with counterions, and solvated

in a TIP3P water box extending at least 10 Å beyond the solute in all directions. Each system underwent a two-stage energy minimization (restrained protein backbone followed by unrestrained minimization), followed by gradual heating from 0 to 300 K over 50 ps under NVT conditions with harmonic restraints on protein heavy atoms. Density equilibration (50 ps) and subsequent NPT equilibration (500 ps) were carried out at 300 K and 1 bar using isotropic position scaling (ntp = 1, taup = 1–2 ps) and a Langevin thermostat (ntt = 3, $\gamma = 2.0\ ps^{-1}$); all bonds involving hydrogen were constrained with SHAKE (ntc = 2, ntf = 2). Production simulations were then run for 100 ns per complex at 300 K and 1 bar with a 2 fs time step, particle-mesh Ewald electrostatics, and an 8.0 Å cutoff for real-space non-bonded interactions, saving coordinates every 10 ps. Structural stability and conformational convergence were evaluated using cpptraj by computing backbone RMSD and per-residue RMSF over the final 50 ns of each trajectory, using the corresponding time-averaged structure as the reference.

Receptor–ligand binding free energies were estimated with both MM-PBSA and MM-GBSA in AmberTools 20 [34], using MMPBSA.py on snapshots extracted every 10 frames (100 ps) from the last 50 ns of each trajectory (startframe = 5000, endframe = 10000, interval = 10). Binding free energies were computed as $\Delta G_bind = \Delta G_complex - (\Delta G_HA + \Delta G_SIA)$, and per-residue energy decomposition analyses were performed to quantify the contribution of individual RBS residues, including positions 145 and 220, to the overall binding free energy for both α2,3- and α2,6-linked receptor analogs [32].

Results

1. Dataset composition and changing host-risk profile

To characterize the global composition of H10Nx viruses, we analyzed 1,045 isolates and summarized their subtype, host family, sampling period, and continental distribution using Sankey visualization (Fig. 1 and Fig. S1). Among the ten subtype combinations, H10N7 was the most prevalent subtype (n = 478, 45.7%), followed by H10N8 (n = 111, 10.6%) and H10N3 (n = 99, 9.5%). Most viruses were detected in North America (n = 661, 63.3%), followed by Asia (n = 243, 23.3%) and Europe (n = 123, 11.8%). Temporally, H10Nx detection increased markedly after 2000, with the periods 2001–2010 (n = 487, 46.6%) and 2011–2023 (n = 499, 47.8%) together accounting for most of the dataset. Host distribution was dominated by wild aquatic birds, especially Anatidae (n = 566, 54.2%) and Scolopacidae (n = 255, 24.4%), whereas infections in Phasianidae (n = 75, 7.2%) increased substantially during the most recent decade. This recent expansion in terrestrial poultry was mainly associated with H10N8, H10N7, and H10N6, while five documented human infections were all recorded in the recent period, collectively suggesting an increasing poultry-associated and zoonotic risk profile for H10Nx viruses. The three most sampled continents accounted for 98.3% of sequences. The remaining 18 isolates were from Africa (n =

9), South America (n = 5), and Oceania (n = 4).

2. Global spatial diffusion is driven by regional persistence rather than intercontinental mixing

Temporal migration analysis of the global dataset revealed that H10Nx circulation was dominated by within-region persistence rather than frequent inter-regional spread (Fig. 2). In Atlantic America, the Atlantic America-to-Atlantic America transition increased sharply after the 1990s and became the predominant transmission pattern, whereas transitions from Atlantic America to East Asia or Pacific America remained much weaker (Fig. 2A). In East Asia, East Asia-to-East Asia transmission rose markedly after 2000 and clearly exceeded transitions from East Asia to Europe and Northeast Asia (Fig. 2B). Europe showed a similar pattern, with Europe-to-Europe transitions increasing substantially from the late 1980s onward, while Europe-to-Africa and Europe-to-Northeast Asia remained relatively limited (Fig. 2C). In Pacific America, the Pacific America-to-Pacific America transition also increased prominently during the late 1990s and 2000s, whereas Pacific America-to-Atlantic America stayed consistently low (Fig. 2D). These results indicate that global H10Nx spread is structured primarily by regional maintenance and amplification, with only low-intensity inter-regional links connecting major transmission systems across the Northern Hemisphere.

3. Global source-sink structure revealed by jump-and-reward analysis

Jump-and-reward analysis further resolved the global source-sink structure of H10Nx circulation at both the host-order and subregional levels (Fig. 3). At the host-order level, Anseriformes showed by far the largest reward value, indicating that this order contributed disproportionately to the long-term maintenance and onward dissemination of H10Nx lineages, whereas Charadriiformes and Galliformes made substantially smaller contributions and mammalian orders remained negligible (Fig. 3A, B). The order-level transition matrix further showed that the most prominent jumps originated from Anseriformes, particularly toward Charadriiformes and Galliformes, supporting the view that waterfowl-associated lineages constitute the major source pool from which H10Nx is redistributed into other avian hosts (Fig. 3A). At the subregional level, Atlantic America displayed the highest reward, followed by East Asia and Europe, whereas Pacific America, Northeast Asia, and especially Africa showed comparatively lower rewards (Fig. 3D). Consistent with this pattern, the strongest subregional jumps were observed from Atlantic America to Pacific America and from East Asia to Northeast Asia, with additional outward connectivity from Europe toward Africa and East Asia (Fig. 3C). Global H10Nx diffusion is thus sustained by a limited number of major avian and geographic source pools, whereas other regions and host groups function predominantly as recipients.

4. Continuous phylogeographic reconstruction of global H10Nx dispersal

To complement the discrete migration analyses, we performed continuous phylogeographic reconstruction of global H10Nx spread using the relaxed random walk (RRW) model implemented in BEAST, which models geographic location as a continuous variable along phylogenetic branches and thus resolves spatial movement at finer geographic resolution than region-level discrete states (Fig. 4). The resulting MCC tree mapped onto a global projection revealed that H10Nx lineages dispersed predominantly within major geographic clusters rather than across continental boundaries, with the densest transmission trajectories concentrated in North America, East Asia, and Europe—consistent with the regional persistence patterns inferred from the discrete MigTime and jump-and-reward analyses (Fig. 4). Intercontinental transmission events were visually sparse in the MCC reconstruction, and where they did occur, they connected regions previously identified as source nodes—particularly between the Atlantic America and East Asia pools and between Europe and Africa—rather than representing diffuse global dissemination (Fig. 4). The RRW reconstruction further indicated that within-region spread was spatially heterogeneous, with lineage trajectories clustering around high-density sampling and avian flyway zones in each major geographic pool, suggesting that local ecological structure, including migratory bird routes and poultry production networks, shapes the fine-scale geographic pattern of H10Nx diffusion (Fig. 4). The continuous reconstruction supports a regionally structured global H10Nx diffusion pattern with only limited long-distance bridges. Given that East Asia—and specifically China—emerged as a major dense trajectory node in the global RRW projection and accounts for all recent zoonotic spillover events, we subsequently scaled our phylogeographic reconstruction to evaluate within-country diffusion dynamics across China.

5. Geographic diffusion dynamics of H10Nx in China

Temporal migration trajectories of the China dataset revealed a clear three-stage shift in the geographic diffusion of H10Nx viruses across the study period (Fig. 5A–D). Before 2000, transmission was concentrated in Hong Kong and the central China provinces of Hubei and Jiangxi, with recurrent within-region persistence in Hong Kong and Hubei accompanied by detectable links from Hong Kong to both Hubei and Jiangxi, indicating that these areas represented the earliest major foci of H10Nx circulation within China (Fig. 5A). During 2000–2010, the migration pattern became centered on Jiangxi, which showed both extensive outward connectivity to multiple provinces and a marked increase in within-province persistence, particularly through strong Jiangxi-to-Jiangxi transmission and repeated links from Jiangxi to Hubei, Hunan, Jiangsu, and Shanghai, consistent with the emergence of Jiangxi as the major dissemination hub during the intermediate phase of expansion (Fig. 5B, C). After 2010, the migration signal progressively shifted eastward, with increasing transitions involving Jiangsu, Shanghai, and Zhejiang, including within-province persistence in Jiangsu and Zhejiang and bidirectional exchange between Jiangsu and Zhejiang, suggesting that the Yangtze River Delta became the dominant center of recent H10Nx spread in China (Fig. 5D). This temporal sequence defines a clear epidemiological shift: the geographic center of gravity for H10Nx circulation in China has progressively migrated from an ancestral Hong Kong–central China focus to a contemporary, highly connected diffusion network in the eastern coastal provinces.

6. Host- and province-level source-sink structure of H10Nx diffusion in China

Jump-and-reward analysis of the China dataset further resolved the source-sink structure of H10Nx circulation at both the host and provincial levels (Fig. 6A–D). At the host level, Anas showed the highest reward and dominated the transition matrix, indicating that duck-associated lineages represented the major reservoir and the major source of onward transmission within China, whereas *Gallus* contributed at a lower but clearly detectable level and mammalian hosts remained marginal recipients in the overall transition network (Fig. 6A, B). These results are consistent with a transmission system centered on sustained circulation within waterfowl, with only limited extension into other hosts, including domestic poultry and occasional mammalian spillover (Fig. 6A, B).

At the provincial level, Jiangxi displayed the highest reward by a clear margin, indicating that it functioned as the major geographic exporter of H10Nx lineages within China (Fig. 6C, D). In contrast, neighboring provinces, particularly Hunan, Hubei, and Fujian, behaved more often as recipient regions, while Hong Kong also remained linked to the broader southern China transmission network rather than acting as the dominant long-term source in the later phase of spread (Fig. 6C, D). Integrating these jump-reward profiles with temporal migration dynamics (Fig. 5) reveals that H10Nx circulation in China relies on Anas-associated maintenance coupled with geographic amplification through a Jiangxi-centered diffusion network.

7. Continuous phylogeographic reconstruction of H10Nx spread in China

Continuous phylogeographic reconstruction of the China dataset using the RRW framework provided spatial support for the discrete geographic patterns inferred from the MigTime and jump-and-reward analyses (Fig. 7). Rather than showing homogeneous diffusion across the country, the MCC reconstruction indicated geographically structured spread, with transmission trajectories concentrated in a limited set of connected regions, consistent with the existence of persistent south-central transmission foci followed by more recent activity in eastern China. In combination with the discrete results, the RRW pattern supports a model in which H10Nx circulation in China was first maintained within the Hong Kong–Hubei–Jiangxi system, subsequently amplified through a Jiangxi-centered diffusion network, and then progressively redistributed toward the eastern coastal provinces, especially Jiangsu, Shanghai, and Zhejiang. These findings therefore reinforce the conclusion that H10Nx spread within China was dominated by regionally clustered persistence and episodic spatial redistribution rather than uniform nationwide dispersal.

8. Host transition dynamics of H10Nx lineages

Temporal reconstruction of host transitions showed that H10Nx circulation was structured around two major host-associated transmission components, namely sustained within-host persistence in *Anas* and subsequent amplification in *Gallus* (Fig. 8A, B). In panel A, the dominant trajectory was Anas-to-Anas transmission, whereas Anas-to-Anser and Anas-to-Gallus transitions were detectable but remained

markedly lower, indicating that duck-associated lineages constituted the primary reservoir from which host expansion occurred (Fig. 8A). In panel B, Gallus-to-Gallus transmission also increased prominently, supporting the role of chickens as an important secondary amplification host once H10Nx entered terrestrial poultry populations (Fig. 8B). Transitions from Gallus to Homo and Sus were present but comparatively limited, suggesting that poultry-associated transmission networks may provide the immediate epidemiological interface for occasional mammalian spillover rather than serving as a major long-term reservoir themselves (Fig. 8B). These results support a stepwise host-diffusion model in which H10Nx is maintained primarily in Anas, expands into Gallus, and only then extends sporadically to mammalian hosts such as humans and swine.

9. Long-term trunk persistence of global & China H10 HA lineages

PACT analysis of the global H10 HA tree showed that long-term lineage persistence was highly uneven across both geographic regions and host groups (Fig. 9A, B). At the geographic level, the trunk was dominated by Atlantic America throughout much of the study period, indicating that this region served as the major long-term reservoir sustaining global H10 HA evolution, whereas East Asia contributed secondarily and other regions appeared to make more limited contributions to trunk continuity (Fig. 9A). At the host level, Anas overwhelmingly occupied the major trunk fraction, consistent with the central role of duck-associated viruses in maintaining the long-term evolutionary backbone of H10Nx circulation (Fig. 9B). The relative contribution of Gallus and Homo increased in more recent years, suggesting that although these hosts did not dominate the historical trunk, they have become increasingly involved in the recent persistence and onward evolution of specific H10 HA lineages (Fig. 9B). The global evolutionary backbone of H10Nx was maintained primarily within Atlantic America and Anas-associated transmission systems, with a more recent extension toward chicken- and human-associated lineages.

PACT analysis of the China H10 HA dataset showed that long-term lineage persistence was strongly concentrated in a limited set of geographic regions and host groups rather than being evenly distributed across the full transmission network (Fig. 10A, B). At the geographic level, Jiangxi dominated the trunk for much of the study period, indicating that this province served as the major long-term reservoir sustaining H10 HA circulation in China (Fig. 10A). In more recent years, the geographic trunk shifted toward eastern coastal provinces, particularly Jiangsu and Zhejiang, consistent with the eastward redistribution pattern inferred from the discrete migration and RRW analyses (Fig. 10A). At the host level, Anas occupied the major trunk fraction throughout most of the temporal window, supporting the view that duck-associated viruses form the enduring evolutionary backbone of H10Nx circulation in China (Fig. 10B). Gallus and Homo became more apparent in the recent part of the host trunk, suggesting that although these hosts were not the historical core of persistence, they have become increasingly involved

in the recent maintenance and onward evolution of specific H10 HA lineages in China (Fig. 10B). These results indicate that long-term H10Nx evolution in China was anchored primarily in Jiangxi- and Anas-associated transmission systems, with more recent extension toward eastern poultry-associated and occasional human-associated lineages.

10. Parallel evolutionary signals associated with recent host expansion

MEME analysis of the whole H10 HA alignment (561 codons; global dN/dS = 0.122) detected 33 sites under episodic positive selection ($p \leq 0.1$). Of these, codon 145 (H3 numbering: 130), located within the receptor-binding site (RBS), showed the strongest signal (LRT = 32.5, $p < 0.0001$), and codon 220 showed only a marginal nominal MEME signal and was therefore treated as an exploratory candidate (LRT = 3.1, $p = 0.10$; 5 branches), consistent with episodic diversification in the 220-loop region that modulates sialic acid receptor preference. FUBAR identified H3 positions 130 (RBS, corresponding to H10 position 145) and 411 (HA2 stalk domain) under pervasive positive selection (Bayes factor > 50). SitePath independently identified H3 positions 130/145 (RBS) and 307/322 (HA1, near cleavage site) as parallel substitution sites (Fig. 11). Branch-level substitution mapping with TreeSub further identified four substitutions — N126D, Q220R, M337I, and I350L — that co-occurred preferentially on branches associated with Gallus host expansion (Fig. S5); among these, Q220R falls directly within the RBS 220-loop and alters the electrostatic environment in a region known to influence avian versus human receptor linkage selectivity, whereas the remaining three map outside the primary binding pocket and may contribute to secondary replication or stability-related adaptation in terrestrial poultry.

11. Receptor-binding energetics associated with HA residue 220 variation

To compare receptor preference across the two modeled systems, total binding free energies were evaluated for the avian-type α2,3-linked receptor analog structure 5TGV and the human-type α2,6-linked receptor analog structure 5TH1. For the α2,3-linked receptor complex, the chicken-background virus showed markedly more favorable binding than the duck-background virus, with MM/GBSA and MM/PBSA free energies of -50.5885 and -10.3261 kcal/mol for chicken versus -17.74 and -0.52 kcal/mol for duck, respectively. For the α2,6-linked receptor complex, MM/GBSA still yielded negative values in both backgrounds (-47.50 kcal/mol for chicken and -31.27 kcal/mol for duck), whereas MM/PBSA returned positive values (4.06 and 6.97 kcal/mol, respectively), indicating that interaction with the human-type receptor was substantially less favorable under the Poisson-Boltzmann-based estimate. Both structural systems support the same qualitative pattern: both modeled viruses showed a stronger predicted association with the avian-type α2,3-linked receptor than with the human-type α2,6-linked receptor, with the chicken-background variant showing higher absolute binding affinities to both receptor types than the duck-background variant. Importantly, because the present analysis does not include a matched wild-type comparator, these data support receptor-binding preference and background-dependent differences, but do

not by themselves isolate the independent contribution of K130Q to the observed binding pattern.

Residue-level energy decomposition of the H10N8 HA--receptor complex refined the structural interpretation of the adaptive sites identified by phylogenetic screening. The H10 numbering convention places the K145Q substitution at the position corresponding to K130Q (H3 numbering, both nomenclatures refer to the same residue in the receptor-binding site). In the avian-type receptor complex (5TGV framework), this 130/145-loop-associated site exhibited a measurable energetic contribution within the binding pocket, confirming its role in modulating local HA-glycan interactions. This localized energetic effect aligns with the substantially stronger overall binding affinity observed for the 220Q background compared with the 220R background in our MM/PBSA calculations, implying that the 130/145 site acts to fine-tune receptor engagement rather than serving as the sole determinant of binding avidity.

Discussion

Our phylogeographic analyses demonstrate that the global evolution of H10Nx is governed by regional persistence rather than frequent intercontinental mixing [2, 10]. The convergence of discrete migration rates, jump-reward estimates, and continuous relaxed-random-walk diffusion patterns supports a structured metapopulation model. In this system, viral lineages remain embedded within geographically confined transmission pools, punctuated only by episodic, long-distance dispersal events [2]. In this respect, H10Nx appears more consistent with the structured persistence described for many low-pathogenic avian influenza viruses in wild birds, where flyway-associated movements allow episodic exchange, but local ecological systems and host communities sustain longer-term lineage maintenance. This pattern is also distinct from the more explosive expansion emphasized in recent studies of clade 2.3.4.4b H5N1, in which rapid large-scale geographic spread has been a defining feature of the ongoing epizootic [35–38]. Ecologically, such a structure is plausible because migratory waterfowl can bridge distant regions, but sustained establishment after introduction is still likely to depend on regional host assemblages, local poultry interfaces, and flyway-constrained ecological connectivity[2, 10]. The central challenge in global H10Nx evolution is therefore identifying which host groups maintain and re-export the virus post-introduction, reinforcing the dominant role of Anseriformes.

At the global scale, our host-transition and PACT analyses identify Anseriformes, particularly *Anas*-associated lineages, as the major maintenance reservoir of H10Nx rather than merely its most frequently sampled host group [2]. This inference is supported by the disproportionate contribution of Anseriformes to both trunk occupancy and outward transition pathways in our dataset, indicating that duck-associated viruses contribute more strongly to long-term lineage persistence and regional

reseeding than other host categories [2]. Recent H10 studies are consistent with this pattern, showing that wild waterfowl dominate the long-term evolutionary background of H10 viruses, whereas mammalian and most poultry-associated H10 lineages are phylogenetically nested within broader avian diversity rather than forming independent, self-sustaining reservoirs[2, 10]. This host asymmetry also aligns with broader avian influenza ecology, in which wild aquatic birds, especially waterfowl, maintain low-pathogenic avian influenza gene pools over long evolutionary timescales and repeatedly seed spillover into domestic bird populations[39]. Mechanistically, this Anseriformes-driven backbone is sustained by their high population density, aquatic habitat overlap, migratory connectivity, and tolerance for asymptomatic LPAIV replication—factors that collectively optimize both local persistence and flyway-scale dispersal [10]. Accordingly, the global phylogeography of H10Nx is best interpreted as a duck-centered evolutionary backbone onto which poultry-associated amplification and occasional mammalian spillover are superimposed, providing the ecological basis for the province-level diffusion patterns observed in China.

Our China-focused phylogeographic analyses suggest that H10Nx transmission within China has not been spatially static but has instead undergone a staged reconfiguration from earlier southern concentration to a more prominent bridging role of Jiangxi and, more recently, stronger activity in the eastern coastal region including the Yangtze River Delta[7]. This geographic shift implies that H10Nx circulation in China is not driven by neutral geographic drift, but rather by the shifting ecological overlap among wild-bird flyways, domestic duck maintenance hubs, and intensive poultry production networks [2, 7]. The intermediate role of Jiangxi is consistent with prior evidence from Poyang Lake, where repeated introductions from migratory waterfowl into domestic ducks were documented over multiple seasons and were subsequently linked to onward movement into live-poultry markets in Nanchang [9]. Jiangxi functions as a critical biological bridge where wild-bird-origin H10 genes are retained, amplified, and reassorted within domestic duck systems prior to spilling over into terrestrial poultry networks [2, 9]. The later strengthening of eastern coastal China is also compatible with recent analyses showing that H10 and N5 reassortant lineages in China are increasingly structured along the East Asian–Australasian flyway and are repeatedly detected in provinces such as Zhejiang, Jiangsu, Shandong, and Liaoning, where migratory connectivity, poultry density, and human exposure opportunities are tightly superimposed [7].

This eastward strengthening should not be interpreted as a purely geographic replacement of southern China, but rather as a redistribution of epidemiological weight toward coastal poultry-production and exchange systems with greater opportunities for amplification and spillover [7]. A similar logic has been observed in other avian influenza subtypes in China, in which initial emergence in the Yangtze River Delta or Pearl River Delta was followed by regional restructuring driven by poultry movement, local persistence, and uneven surveillance intensity rather than by a single persistent epicenter [16]. Accordingly, the key implication of the Chinese H10Nx spatial shift is not the map pattern itself, but the increasing overlap between transmission hubs and poultry-associated human exposure interfaces, which sets up the host-jump dynamics discussed in the next section.

Our host-transition analyses suggest that H10Nx evolution is still anchored in duck-associated maintenance networks, whereas terrestrial poultry, particularly the recent rise in Phasianidae with a chicken-centered amplification interface, likely function as secondary amplification and bridge hosts once the virus enters poultry production systems. This interpretation is consistent with recent virological studies showing that human-associated H10N3 and H10N5 viruses in China were genetically linked to avian lineages circulating in poultry or wild bird–poultry systems, rather than representing established human-adapted lineages [11, 40, 41]. The recent expansion of H10Nx within Phasianidae, temporally coinciding with all documented human H10 spillover events, suggests that the most epidemiologically consequential shift in H10Nx evolution is the strengthening of the duck-chicken-human interface, rather than the acquisition of intrinsic human transmissibility. This cautious interpretation is consistent with WHO guidance indicating that zoonotic influenza infections are primarily associated with direct or indirect exposure to infected birds or contaminated environments, including live bird markets, and that currently circulating zoonotic influenza viruses have not demonstrated sustained human-to-human transmission. Within this framework, China appears especially important not simply because cases were detected there, but because multiple human H10 events have been tied to poultry-associated exposure settings, including the fatal H10N8 case linked to live poultry market exposure, the broader live-poultry-market circulation and reassortment history of H10N3 viruses, and the first human H10N5 case associated with exposure to infected duck products or live poultry [8, 11, 42, 43]. Therefore, the present zoonotic risk of H10Nx is fundamentally an interface-driven spillover problem, emerging from the convergence of waterfowl maintenance, poultry amplification, and intensive human exposure opportunities, especially in China, rather than as evidence that H10Nx has already crossed into stable human adaptation. This view is also consistent with experimental work showing that recent human-isolated H10N5 viruses can infect mammals and display dual receptor-binding characteristics with a stronger avian preference, yet have not demonstrated transmission in guinea pigs [41].

Our results suggest that the recent host expansion of H10Nx was accompanied by repeated amino-acid changes in and around the HA receptor-binding region, but the current evidence supports incremental tuning rather than a completed switch to human adaptation. The H10 HA numbering convention places the K145Q substitution at the position corresponding to K130Q in H3 numbering; both nomenclatures refer to the same residue in the receptor-binding site, so this represents one recurrent change rather than two independent lines of evidence. Structural studies of H10 HA support this conservative view by showing that H10 viruses can display measurable interaction with human-type glycans while still retaining an overall preference for avian receptors, indicating that partial zoonotic compatibility and fully human-adapted receptor usage are not equivalent states [9, 44, 45]. Within this framework, the importance of the 130/145-equivalent site

lies less in proving a stand-alone human-adapting mutation than in its location adjacent to the receptor-binding pocket, where residues on the 130-loop can influence glycan positioning and local interaction geometry during receptor engagement [9, 44]. This interpretation is also compatible with the residue-level energetic analysis presented here, in which the 130/145 site showed an interpretable contribution but did not account for the much larger background-dependent difference observed between the 220Q and 220R receptor-binding contexts. By contrast, both previous H10 structural work and recent H10N5 analyses indicate that the 220-loop background likely exerts a broader effect on binding avidity, because residues around positions 221–226 help shape loop conformation, receptor trajectory, and the balance between avian- and human-type receptor accommodation [41, 44, 46]. Recent H10N5 data showed dual-receptor binding with a stronger avian preference and again pointed to combined effects of the 130-loop and 220-loop, rather than a single deterministic substitution, in modulating human-type receptor engagement [41]. More broadly, this pattern remains consistent with established influenza receptor-adaptation logic, in which remodeling of the 220-loop has been central to major host-range shifts in other subtypes, whereas contemporary H10 viruses still largely retain avian-signature receptor-binding features [10, 41, 44–46]. The K130Q (K145Q)-equivalent change likely acts as a context-dependent convergent fine-tuning site modulated by the 220-loop background. Residue 411, located in the HA2 stalk domain, lacks direct structural evidence for receptor-binding effects. Ultimately, recent H10Nx evolution reflects gradual structural optimization within an avian-biased binding framework. This explains how sporadic spillover into humans can repeatedly occur without requiring a definitive, pandemic-like human-adaptation switch [41, 45, 46].

Several limitations should be considered when interpreting our findings. 1. The global H10Nx sequence pool is inevitably shaped by substantial heterogeneity in surveillance intensity across regions, years, and host groups, which can influence the apparent strength of source-sink structure, trunk persistence, and inferred diffusion pathways [2, 4]. 2. Phylogeographic reconstructions remain sensitive to metadata quality, including date completion, geographic discretization, and coordinate precision, so inferred migration histories should be interpreted as probabilistic reconstructions rather than literal transmission maps [2]. 3. Host-transition analyses based on ancestral-state inference do not directly observe transmission chains and therefore cannot by themselves prove the exact epidemiological sequence of spillover events between ducks, chickens, and humans [4, 47]. 4. Our structural and binding-energy analyses provide hypothesis-supporting evidence for receptor-binding optimization, but they do not substitute for reverse genetics, glycan-binding, or transmission experiments, and therefore should not be overinterpreted as proof of completed human adaptation [12, 48]. 5. Geographic source-sink estimates are derived from Bayesian ancestral-state reconstruction and reflect the posterior probability distribution of geographic states at internal nodes

given tip observations; these estimates are inherently sensitive to sampling representation across geographic states. 6. The six-region geographic discretization was defined by K-means clustering on longitude-latitude coordinates to achieve approximately equal sequence counts across states, an approach that maximizes computational tractability but may not correspond to biologically or epidemiologically meaningful geographic boundaries. 7. The human host category contained only five sequences in the analyzed dataset, making ancestral-state estimates for this category highly uncertain and limiting the resolution of host-transition inferences involving human hosts.

Despite these constraints, the main epidemiological signal is internally consistent across multiple analytical layers. When considered together with recent evidence that H10 viruses continue to cause sporadic human infections without evidence of sustained human-to-human transmission, our results support the view that the current public-health concern is an increase in spillover opportunity rather than the emergence of an already human-adapted epidemic lineage [12, 48]. From a surveillance perspective, these findings argue for shifting monitoring upstream to the full duck-reservoir–chicken-amplification–human-exposure continuum, rather than relying primarily on detection after human cases appear [2, 4]. In practical terms, priority should be given to coordinated sampling of wild waterfowl and domestic ducks, intensified virological surveillance in chickens and live-poultry-market environments, and prospective tracking of recently expanding H10 lineages and candidate HA adaptive markers within a One Health framework [12, 47]. Accordingly, H10Nx must be categorized as a zoonotic lineage with an intensifying interface risk profile. Jiangxi Province should be prioritized for longitudinal duck–chicken interface sampling, given its role as the dominant source province (79 out-migration events). The most critical intervention window remains upstream: integrated One Health surveillance at the wildlife-poultry-human boundary before the virus acquires efficient human transmission.

Funding

This work was supported by the Natural Science Foundation Reserve Project of Jiangsu Agri-animal Husbandry Vocational College, awarded to Dongchang He (NSF2023CB15); the Poultry Disease Prevention and Control Team Project of Jiangsu Agri-animal Husbandry Vocational College, led by Professor Yongjuan Wang (NSF2024TC01); the Open Project Program of Jiangsu Key Laboratory of Zoonosis (R2410); and the Major Project of Natural Science Research in Universities of Jiangsu Province, “Molecular Evolution and Pathogenic Mechanisms of Swine Influenza Virus” (23KJA230003).

Acknowledgment

Computing resources used in this study were provided by the Information Technology Center of Jiangsu Agri-animal Husbandry Vocational College.

Data Availability

All sequence data analysed in this study were obtained from the GISAID EpiFlu™ database (https://www.gisaid.org).

Declarations

Ethics approval and consent to participate: Not applicable.

Consent for publication: Not applicable.

Competing interests: The authors declare no competing interests.

1. Wang Y, Wang M, Zhang H, et al (2022) Emergence, Evolution, and Biological Characteristics of H10N4 and H10N8 Avian Influenza Viruses in Migratory Wild Birds Detected in Eastern China in 2020. Microbiol Spectr 10:e00807-22. https://doi.org/10.1128/spectrum.00807-22

2. Lv X, Tian J, Li X, et al (2023) H10Nx avian influenza viruses detected in wild birds in China pose potential threat to mammals. One Health 16:100515. https://doi.org/10.1016/j.onehlt.2023.100515

3. Sutton TC, Lamirande EW, Czako R, Subbarao K (2017) Evaluation of the Biological Properties and Cross-Reactive Antibody Response to H10 Influenza Viruses in Ferrets. J Virol 91:e00895-17. https://doi.org/10.1128/jvi.00895-17

4. Everest H, Billington E, Daines R, et al (2021) The Emergence and Zoonotic Transmission of H10Nx Avian Influenza Virus Infections. mBio 12:e01785-21. https://doi.org/10.1128/mbio.01785-21

5. Arzey GG, Kirkland PD, Arzey KE, et al Influenza virus a (H10N7) in chickens and poultry abattoir workers, australia - volume 18, number 5—may 2012 - emerging infectious diseases journal - CDC. https://doi.org/10.3201/eid1805.111852

6. Chen H, Yuan H, Gao R, et al (2014) Clinical and epidemiological characteristics of a fatal case of avian influenza A H10N8 virus infection: a descriptive study. The Lancet 383:714–721. https://doi.org/10.1016/S0140-6736(14)60111-2

7. Chen W, Lu S, Xiong H, et al (2025) Gene flow and its sporadic spillover: H10 and N5 avian influenza viruses from wild birds and the H10N5 human cases in China. Virologica Sinica 40:15–23. https://doi.org/10.1016/j.virs.2024.12.002

8. Qi X, Qiu H, Hao S, et al (2022) Human Infection with an Avian-Origin Influenza A (H10N3) Virus. N Engl J Med 386:1087–1088. https://doi.org/10.1056/NEJMc2112416

9. Ma C, Lam TT-Y, Chai Y, et al (2015) Emergence and Evolution of H10 Subtype Influenza Viruses in Poultry in China. J Virol 89:3534–3541. https://doi.org/10.1128/jvi.03167-14

10. Li W-C, Chang C-Y, Liu Y-P, et al (2025) Intensive reassortment and frequent intercontinental transmission revealed by long-term genetic analysis of H10 avian influenza viruses in Taiwan. Emerging Microbes & Infections 14:2556794. https://doi.org/10.1080/22221751.2025.2556794

11. Wu J, Zhang X, Zhao Y, et al (2025) North American-origin influenza A (H10) viruses in Eurasian wild birds (2022–2024): implications for the emergence of human H10N5 virus. Emerging Microbes & Infections 14:2465308. https://doi.org/10.1080/22221751.2025.2465308

12. Yang J, Zheng S, Sun J, et al (2025) A human-infecting H10N5 avian influenza virus: Clinical features, virus reassortment, receptor-binding affinity, and possible transmission routes. Journal of Infection 90:106456. https://doi.org/10.1016/j.jinf.2025.106456

13. Lemey P, Rambaut A, Drummond AJ, Suchard MA (2009) Bayesian phylogeography finds its roots. PLoS Comput Biol 5:e1000520. https://doi.org/10.1371/journal.pcbi.1000520

14. He D, Gu J, Gu M, et al (2021) Genetic and antigenic diversity of H7N9 highly pathogenic avian influenza virus in china. Infect genet evol : j mol epidemiol evol genet infect dis 93:104993. https://doi.org/10.1016/j.meegid.2021.104993

15. Zhou Z-J, Qiu Y, Pu Y, et al (2020) BioAider: an efficient tool for viral genome analysis and its application in tracing SARS-CoV-2 transmission. Sustainable Cities Soc 63:102466. https://doi.org/10.1016/j.scs.2020.102466

16. He D, Gu M, Wang X, et al (2021) Spatiotemporal associations and molecular evolution of highly pathogenic avian influenza a H7N9 virus in china from 2017 to 2021. Viruses 13:2524. https://doi.org/10.3390/v13122524

17. Zhang D, Gao F, Jakovlić I, et al (2020) PhyloSuite: an integrated and scalable desktop platform for streamlined molecular sequence data management and evolutionary phylogenetics studies. Mol Ecol Resour 20:348–355. https://doi.org/10.1111/1755-0998.13096

18. Minh BQ, Schmidt HA, Chernomor O, et al (2020) IQ-TREE 2: new models and efficient

methods for phylogenetic inference in the genomic era. Mol Biol Evol 37:1530–1534. https://doi.org/10.1093/molbev/msaa015

19. Kalyaanamoorthy S, Minh BQ, Wong TKF, et al (2017) ModelFinder: fast model selection for accurate phylogenetic estimates. Nat Methods 14:587–589. https://doi.org/10.1038/nmeth.4285

20. Xu S, Dai Z, Guo P, et al (2021) ggtreeExtra: compact visualization of richly annotated phylogenetic data. Mol Biol Evol 38:4039–4042. https://doi.org/10.1093/molbev/msab166

21. Yu G (2020) Using ggtree to visualize data on tree-like structures. Curr protoc bioinform 69:96. https://doi.org/10.1002/cpbi.96

22. Sagulenko P, Puller V, Neher RA (2018) TreeTime: maximum-likelihood phylodynamic analysis. Virus Evol 4:42. https://doi.org/10.1093/ve/vex042

23. Hill V, Baele G (2019) Bayesian estimation of past population dynamics in BEAST 1.10 using the skygrid coalescent model. Mol Biol Evol 36:2620–2628. https://doi.org/10.1093/molbev/msz172

24. Brynildsrud OB, Pepperell CS, Suffys P, et al (2018) Global expansion of mycobacterium tuberculosis lineage 4 shaped by colonial migration and local adaptation. Sci Adv 4:eaat5869. https://doi.org/10.1126/sciadv.aat5869

25. Dellicour S, Gill MS, Faria NR, et al (2021) Relax, keep walking - a practical guide to continuous phylogeographic inference with BEAST. Mol Biol Evol 38:3486–3493. https://doi.org/10.1093/molbev/msab031

26. Dellicour S, Baele G, Dudas G, et al (2018) Phylodynamic assessment of intervention strategies for the west african ebola virus outbreak. Nat Commun 9:2222. https://doi.org/10.1038/s41467-018-03763-2

27. Dellicour S, Faria NR, Rose R, et al (2026) SERAPHIM 2.0: an extended toolbox for studying phylogenetically informed movements. Bioinformatics btag093. https://doi.org/10.1093/bioinformatics/btag093

28. Murrell B, Wertheim JO, Moola S, et al (2012) Detecting individual sites subject to episodic diversifying selection. PLos Genet 8:1002764. https://doi.org/10.1371/journal.pgen.1002764

29. Murrell B, Moola S, Mabona A, et al (2013) FUBAR: a fast, unconstrained bayesian approximation for inferring selection. Mol Biol Evol 30:1196–205. https://doi.org/10.1093/molbev/mst030

30. Wang L-G, Lam TT-Y, Xu S, et al (2020) Treeio: an R package for phylogenetic tree input and output with richly annotated and associated data. Mol Biol Evol 37:599–603. https://doi.org/10.1093/molbev/msz240

31. Ji C, Han N, Cheng Y, et al (2022) sitePath: A visual tool to identify polymorphism clades and help find fixed and parallel mutations. BMC Bioinf 23:504. https://doi.org/10.1186/s12859-022-05064-4

32. Salomon-Ferrer R, Case DA, Walker RC (2013) An overview of the amber biomolecular simulation package. Wiley Interdiscip Rev: Comput Mol Sci 3:198–210. https://doi.org/10.1002/wcms.1121

33. Tzarum N, Vries RP, Peng W, et al (2017) The 150-loop restricts the host specificity of human H10N8 influenza virus. Cell Rep 19:235–245. https://doi.org/10.1016/j.celrep.2017.03.054

34. Genheden S, Ryde U (2015) The MM/PBSA and MM/GBSA methods to estimate ligand-binding affinities. Expert Opin Drug Discovery 10:449–61. https://doi.org/10.1517/17460441.2015.1032936

35. Damodaran L, Jaeger AS, Moncla LH (2026) Ecology and spread of the north American H5N1 epizootic. Nature 649:432–441. https://doi.org/10.1038/s41586-025-09737-x

36. Rivetti AV, Reischak D, de Oliveira CHS, et al (2024) Phylodynamics of avian influenza a(H5N1) viruses from outbreaks in Brazil. Virus Res 347:199415. https://doi.org/10.1016/j.virusres.2024.199415

37. Koopmans MPG, Behravesh CB, Cunningham AA, et al (2024) The panzootic spread of highly pathogenic avian influenza H5N1 sublineage 2.3.4.4b: A critical appraisal of one health preparedness and prevention. The Lancet Infectious Diseases 24:e774–e781. https://doi.org/10.1016/S1473-3099(24)00438-9

38. Halwe NJ, Cool K, Breithaupt A, et al (2025) H5N1 clade 2.3.4.4b dynamics in experimentally infected calves and cows. Nature 637:903–912. https://doi.org/10.1038/s41586-024-08063-y

39. Authority (EFSA) EFS, Abrahantes JC, Aznar I, et al (2025) Avian influenza annual report 2023. EFSA J 23:e9197. https://doi.org/10.2903/j.efsa.2025.9197

40. Zhang Y, Shi J, Cui P, et al (2023) Genetic analysis and biological characterization of H10N3 influenza a viruses isolated in china from 2014 to 2021. J Med Virol 95:e28476. https://doi.org/10.1002/jmv.28476

41. Hao M, Wu J, Ji L, et al (2025) Pathogenicity, transmissibility, and receptor binding of a

human-isolated influenza A (H10N5) virus. mBio 16:e00731-25. https://doi.org/10.1128/mbio.00731-25

42. Lai C-C, Hsueh P-R (2024) Human infection caused by avian influenza A (H10N5) virus. Journal of Microbiology, Immunology and Infection 57:343–345. https://doi.org/10.1016/j.jmii.2024.04.006

43. To KKW, Tsang AKL, Chan JFW, et al (2014) Emergence in China of human disease due to avian influenza A(H10N8) – Cause for concern? Journal of Infection 68:205–215. https://doi.org/10.1016/j.jinf.2013.12.014

44. Vachieri SG, Xiong X, Collins PJ, et al (2014) Receptor binding by H10 influenza viruses. Nature 511:475–477. https://doi.org/10.1038/nature13443

45. Yang H, Carney PJ, Chang JC, et al (2015) Structure and Receptor Binding Preferences of Recombinant Hemagglutinins from Avian and Human H6 and H10 Influenza A Virus Subtypes. J Virol 89:4612–4623. https://doi.org/10.1128/jvi.03456-14

46. Wang M, Zhang W, Qi J, et al (2015) Structural basis for preferential avian receptor binding by the human-infecting H10N8 avian influenza virus. Nat Commun 6:5600. https://doi.org/10.1038/ncomms6600

47. Liu K, Wang X, Sun Y, et al (2025) Will avian influenza virus (H10N3) cause a major public health threat? Animals and Zoonoses S2950248925000847. https://doi.org/10.1016/j.azn.2025.11.003

48. Liu K, Qi X, Bao C, et al (2024) Novel H10N3 avian influenza viruses: a potential threat to public health. Lancet Microbe 5:e417. https://doi.org/10.1016/S2666-5247(23)00409-3

Fig. 1 Global composition of H10Nx viruses by subtype, host family, sampling period, and continent. Sankey diagram summarizing the subtype, host-family, sampling-period, and

continental composition of 1,045 non-redundant H10Nx viruses. Flows connect viral subtype, host family, sampling period, and continent of isolation; node width is proportional to the number of strains. The diagram shows the dominance of H10N7, the major contribution of wild aquatic bird families, especially Anatidae and Scolopacidae, and the marked increase in detections after 2000. The recent rise of H10N8-, H10N7-, and H10N6-associated detections in terrestrial poultry temporally coincides with the period in which all documented human infections were reported.

Fig. 2 Time-varying regional migration dynamics of global H10Nx lineages. Temporal migration trajectories of the global H10Nx dataset inferred from the time-scaled MCC tree. Panels show annually resolved transition counts involving major geographic regions, allowing comparison between within-region persistence and inter-regional spread. Atlantic America, East Asia, Europe, and Pacific America each showed increases in region-to-itself transitions through time, whereas cross-regional links remained comparatively limited.

Fig. 3 Global source-sink structure of H10Nx circulation inferred from jump-and-reward analysis. Jump-and-reward analysis of the global H10Nx dataset at the host-order and subregional levels. Panels A and B summarize host-order transitions and reward values, respectively; Anseriformes occupies the largest share in both summaries. Panels C and D summarize subregional transition intensity and reward values, with Atlantic America showing the largest contribution, followed by East Asia and Europe.

Fig. 4 Continuous phylogeographic reconstruction of global H10Nx diffusion. Maximum clade credibility tree of the global H10Nx HA dataset projected in continuous geographic space under a Cauchy relaxed random walk (RRW) model. Branch trajectories represent inferred lineage dispersal through time based on country-level centroid coordinates. The reconstruction shows that most lineage movement was concentrated within major geographic clusters, especially North America, East Asia, and Europe, whereas long-distance intercontinental dispersal was comparatively infrequent.

Fig. 5 Temporal geographic diffusion dynamics of H10Nx viruses within China. Time-resolved migration analysis of the China dataset based on the MCC tree and annual transition counting.

The figure illustrates a stepwise shift in the geographic focus of H10Nx spread, from an early Hong Kong--Hubei--Jiangxi system to an intermediate Jiangxi-centered phase and then to a more recent eastern coastal focus involving Jiangsu, Shanghai, and Zhejiang. Strong within-province persistence is visible in the major focal areas during different time periods.

Fig. 6 Host- and province-level source-sink structure of H10Nx diffusion in China. Jump-and-reward analysis of the China H10Nx dataset at the host and provincial levels. Panels A and B show that Anas-associated lineages dominated the host transition matrix and reward distribution. Panels C and D show that Jiangxi had the highest provincial reward and occupied a central position in the province-to-province diffusion network.

Fig. 7 Continuous phylogeographic reconstruction of H10Nx spread in China. Maximum clade credibility tree of the China H10Nx dataset projected in continuous geographic space under the relaxed random walk (RRW) model. Branch trajectories were inferred using province-level centroid coordinates to resolve within-China dispersal. The reconstruction shows geographically clustered spread rather than homogeneous nationwide diffusion, with persistent activity in south-central China followed by more recent concentration in the eastern coastal region. These patterns are concordant with the discrete migration results shown in Figs. 5 and 6.

Fig. 8 Temporal host transition dynamics of H10Nx lineages. Time-resolved host transition trajectories reconstructed from the host-annotated H10Nx MCC tree. The dominant component of host diffusion was sustained Anas-to-Anas transition, indicating that duck-associated viruses formed the primary reservoir. Gallus-to-Gallus transition also increased through time. In contrast, transitions from poultry to mammalian hosts (Homo and Sus) were detectable but limited.

Fig. 9 Long-term trunk persistence of global H10 HA lineages across regions and hosts. PACT skyline analysis of the global H10 HA posterior tree distribution. Panel A shows the relative contribution of geographic regions to the long-term trunk, with Atlantic America contributing the largest fraction and East Asia contributing secondarily. Panel B shows the host composition of the trunk, with *Anas* dominating much of the evolutionary backbone and more recent increases in the contribution of Gallus- and Homo-associated lineages.

Fig. 10 Long-term trunk persistence of China H10 HA lineages across provinces and hosts. PACT skyline analysis of the China H10 HA posterior tree distribution. Panel A shows the relative contribution of provinces to the long-term trunk, with Jiangxi dominating much of the historical signal and more recent contributions from eastern coastal provinces, especially Jiangsu and Zhejiang. Panel B shows the host composition of the trunk, in which Anas remained the dominant long-term backbone, whereas *Gallus* and *Homo* became more apparent in recent years.

Fig. 11 Parallel amino acid evolution in the global H10 HA phylogeny. SitePath analysis identified residues 130 (H3 numbering; H10: 145) and 307 (H3; H10: 322) as sites showing evidence of parallel evolution.

Fig. 12 Residue-level receptor-binding energetics of the H10N8 HA–sialic acid complex. Binding free-energy analysis and residue decomposition were used to evaluate receptor-binding energetics in modeled H10N8 HA--sialic acid complexes. Total free-energy estimates showed that both modeled viral backgrounds bound the avian-type α2,3-linked receptor analog more favorably than the human-type α2,6-linked analog. Residue-level decomposition showed cooperative energetic contributions from multiple neighboring residues within the receptor-binding pocket.

Supplementary Materials Results

Fig. S1. Distribution of global H10Nx viruses across continents, host orders, and subtypes.

Supplementary Sankey diagram showing the global composition of H10Nx viruses at the host-order level. Most viruses were sampled in North America and Asia and originated predominantly from avian orders, especially *Anseriformes* and *Charadriiformes*, followed by *Galliformes*. Mammalian detections were rare and included only occasional records from primates, carnivores, and artiodactyls. Among subtypes, H10N7 was the most prevalent, followed by H10N8 and H10N3.

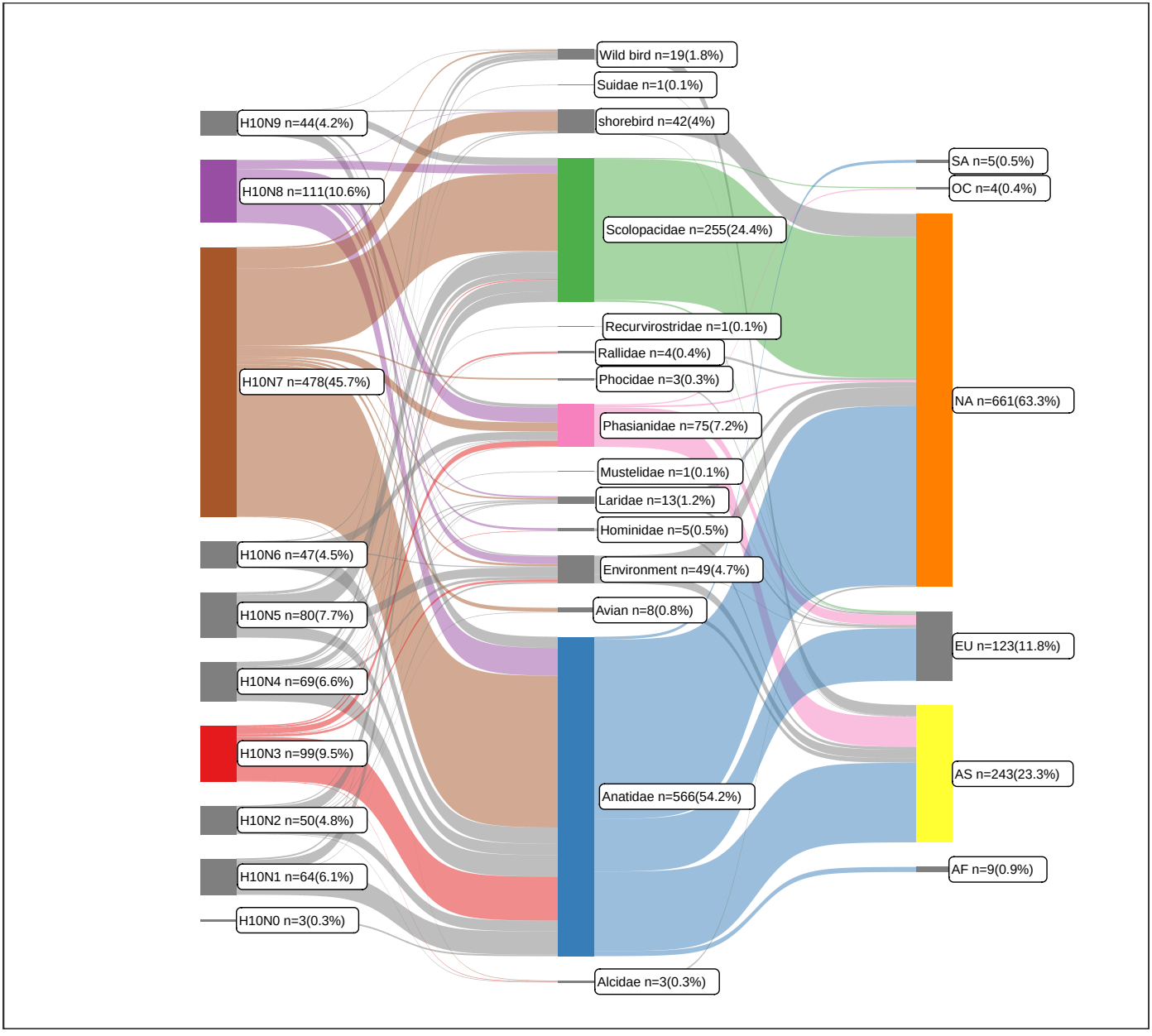
Fig. S2. Temporal signal and molecular clock evaluation of the global H10 HA dataset**.** Prior to

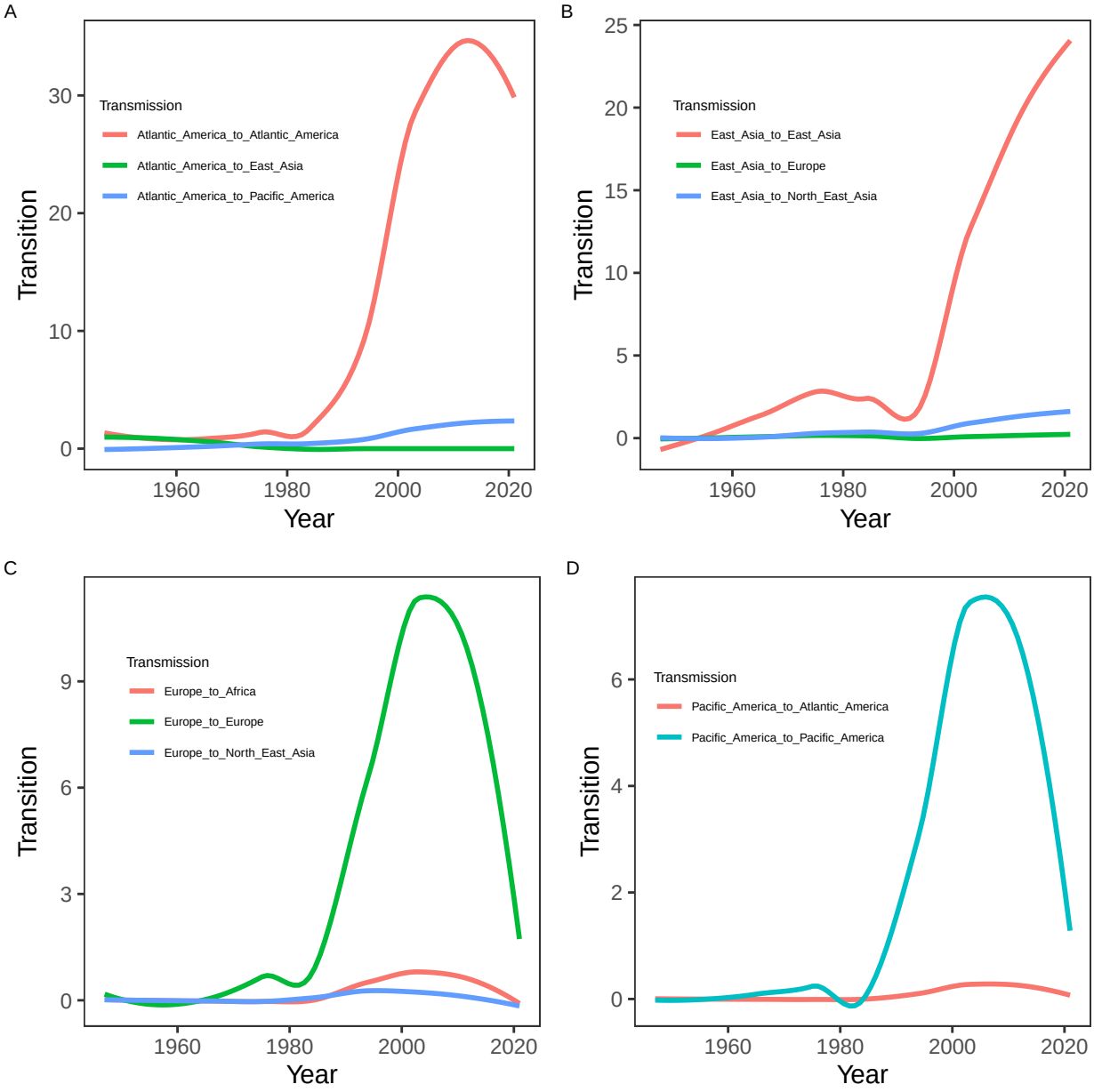
Bayesian phylodynamic analysis, the temporal signal of the H10 HA dataset was evaluated by TreeTime root-to-tip regression. Root-to-tip distance showed a positive linear correlation with sampling date, yielding an estimated substitution rate (β) of 3.75×10^{-3} substitutions per site per year. Extrapolation of the regression line placed the root date at approximately 1921.5. Sequences deviating substantially from the regression line were treated as clock outliers (red points) and excluded prior to BEAST analysis.

Fig. S3. Historical population dynamics of the global H10Nx HA gene pool. B Bayesian skyline plot of the global H10Nx HA dataset reconstructed in BEAST. The median effective population size remained broadly stable over much of the inferred history, although uncertainty was wider in the earlier period. A moderate increase in relative genetic diversity was observed after 2000.

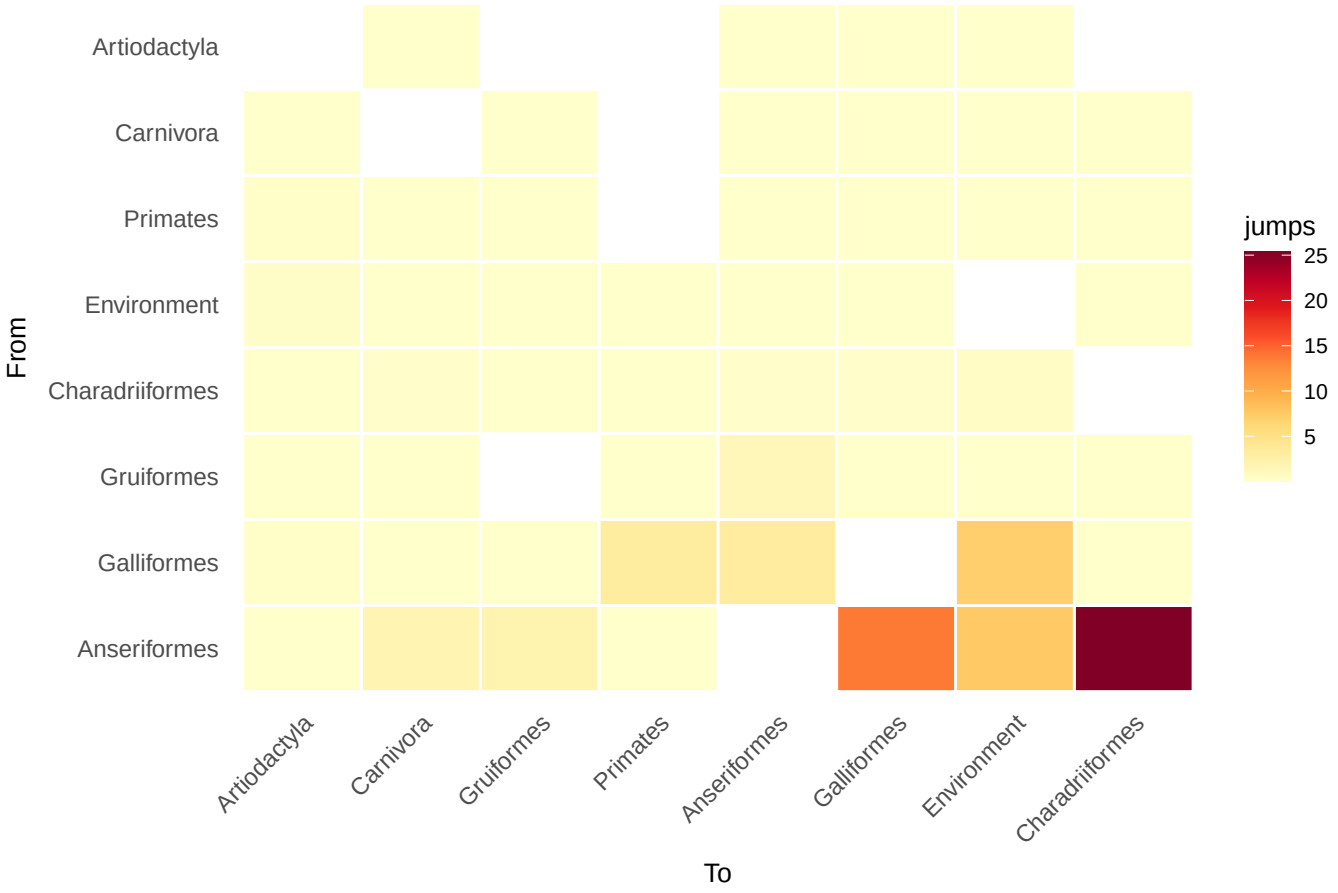
Fig. S4. Geographic clustering framework for global H10Nx phylogeographic analysis. Sampling localities of the global H10Nx dataset used for discrete phylogeographic analysis were geocoded and grouped by K-means clustering to define operational regions. Initial clustering was performed with k = 8, after which two clusters were excluded: an Iceland cluster showing disproportionate sampling density relative to geographic area and an Oceania cluster represented by a single sequence. The remaining six clusters were retained as Africa, Europe, East Asia, Northeast Asia, Atlantic America, and Pacific America.

Fig. S5. Amino acid substitutions mapped on the global H10 HA phylogeny. Ancestral-state reconstruction of amino acid substitutions mapped onto the global H10 HA phylogeny using TreeSub. Representative substitutions included N126D, Q220R, M337I, and I350L, spanning both receptor-associated and non-receptor-associated regions of the protein. Among these sites, residue 220 lies in the receptor-binding-related region. This figure provides the broader phylogenetic context for the site-focused analyses presented in Fig. 11 and Fig. 12.

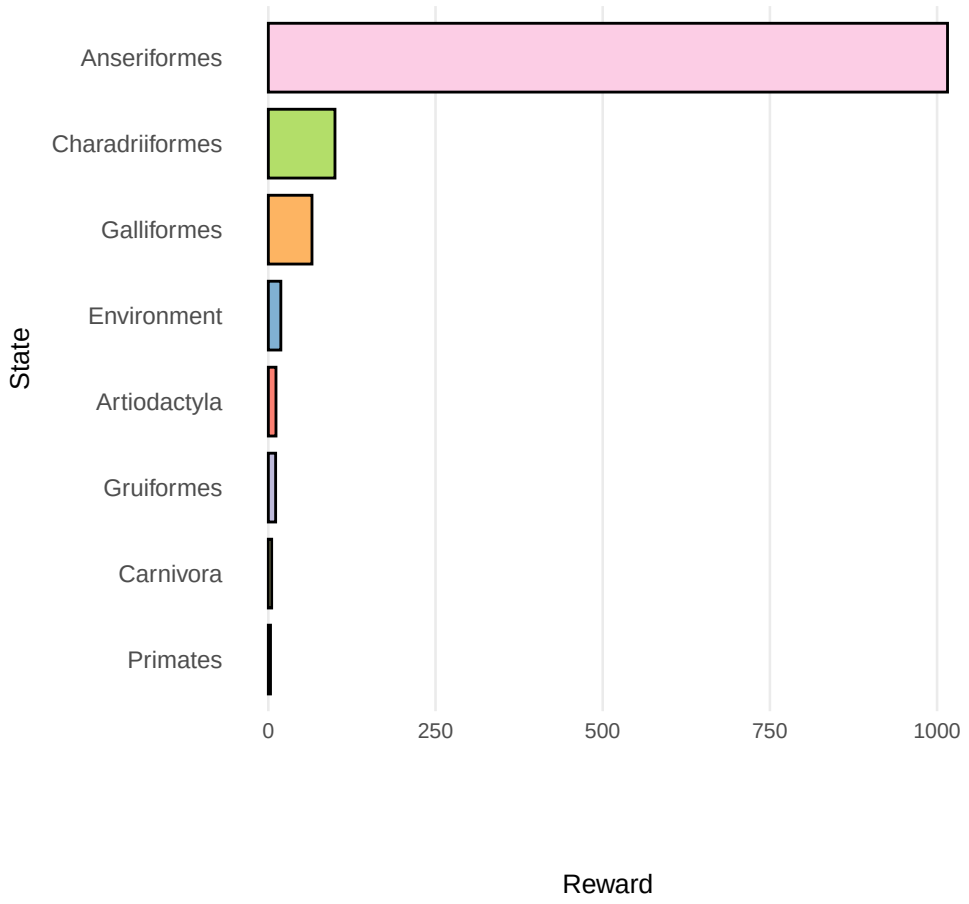

Wild bird n=19(1.8%)
Suidae n=1(0.1%)
shorebird n=42(4%)
Scolopacidae n=255(24.4%)
Recurvirostridae n=1(0.1%)
Rallidae n=4(0.4%)
Phocidae n=3(0.3%)
Phasianidae n=75(7.2%)
Mustelidae n=1(0.1%)
Laridae n=13(1.2%)
Hominidae n=5(0.5%)
Environment n=49(4.7%)
Avian n=8(0.8%)
Anatidae n=566(54.2%)
Alcidae n=3(0.3%)
H10N9 n=44(4.2%)
H10N8 n=111(10.6%)
H10N7 n=478(45.7%)
H10N6 n=47(4.5%)
H10N5 n=80(7.7%)
H10N4 n=69(6.6%)
H10N3 n=99(9.5%)
H10N2 n=50(4.8%)
H10N1 n=64(6.1%)
H10N0 n=3(0.3%)
SA n=5(0.5%)
OC n=4(0.4%)
NA n=661(63.3%)
EU n=123(11.8%)
AS n=243(23.3%)
AF n=9(0.9%)
Subtype
Family
Continent


A
Transmission
Atlantic_America_to_Atlantic_America
Atlantic_America_to_East_Asia
Atlantic_America_to_Pacific_America
Transition
Year
B
Transmission
East_Asia_to_East_Asia
East_Asia_to_Europe
East_Asia_to_North_East_Asia
Transition
Year
C
Transmission
Europe_to_Africa
Europe_to_Europe
Europe_to_North_East_Asia
Transition
Year
D
Transmission
Pacific_America_to_Atlantic_America
Pacific_America_to_Pacific_America
Transition
Year

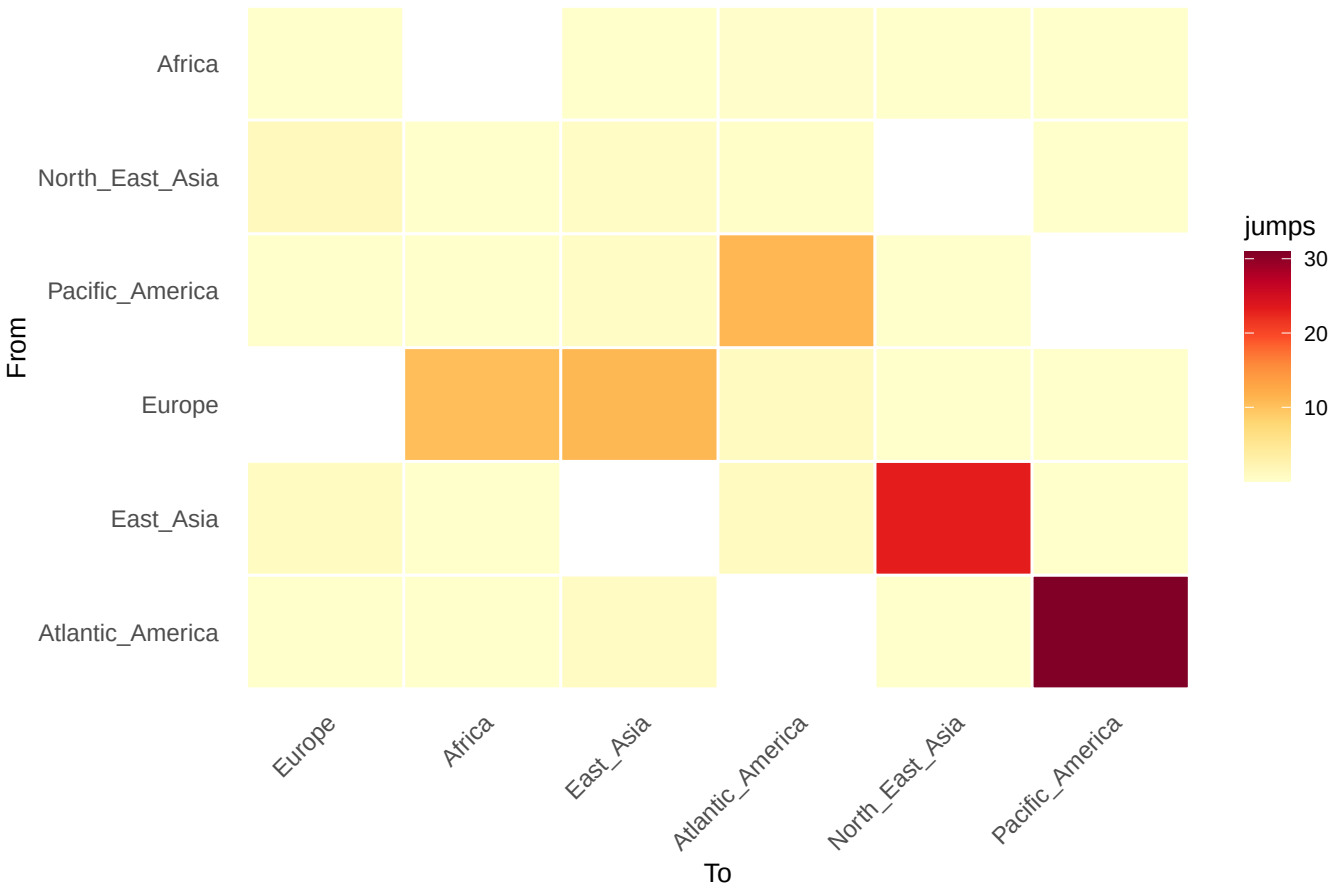
A. Order−level transitions



B. Order−level rewards



C. Subregion transitions



D. Subregion rewards

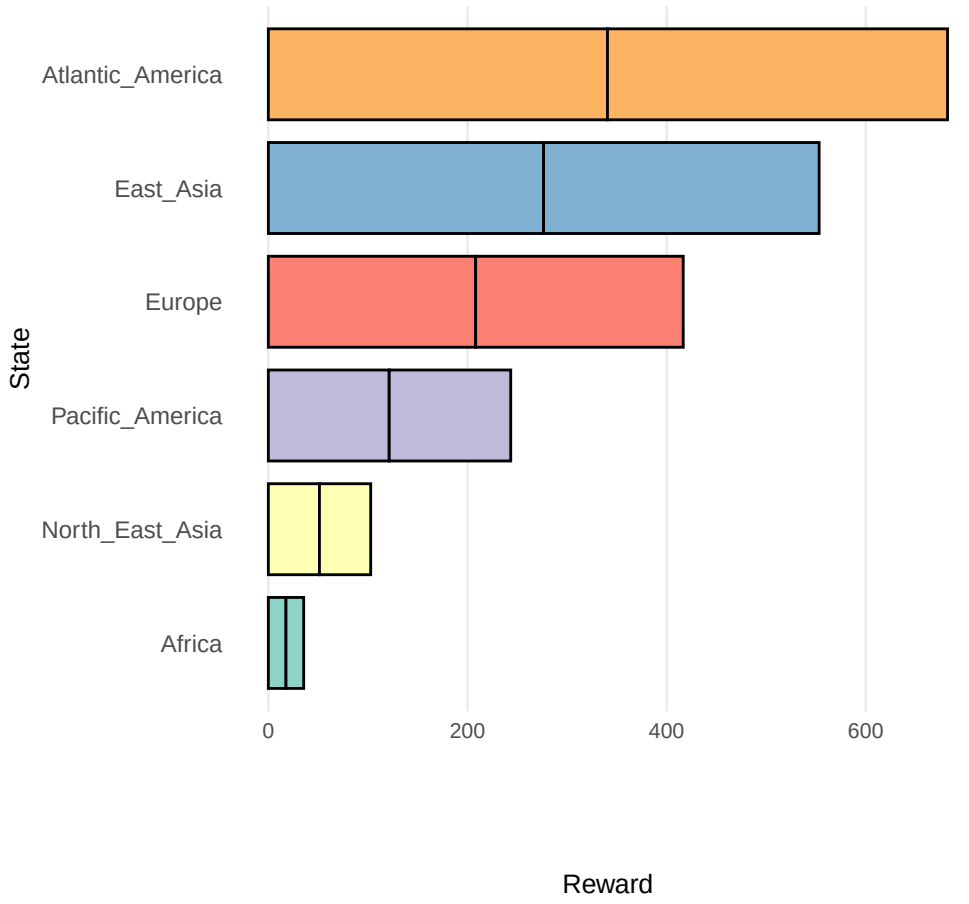
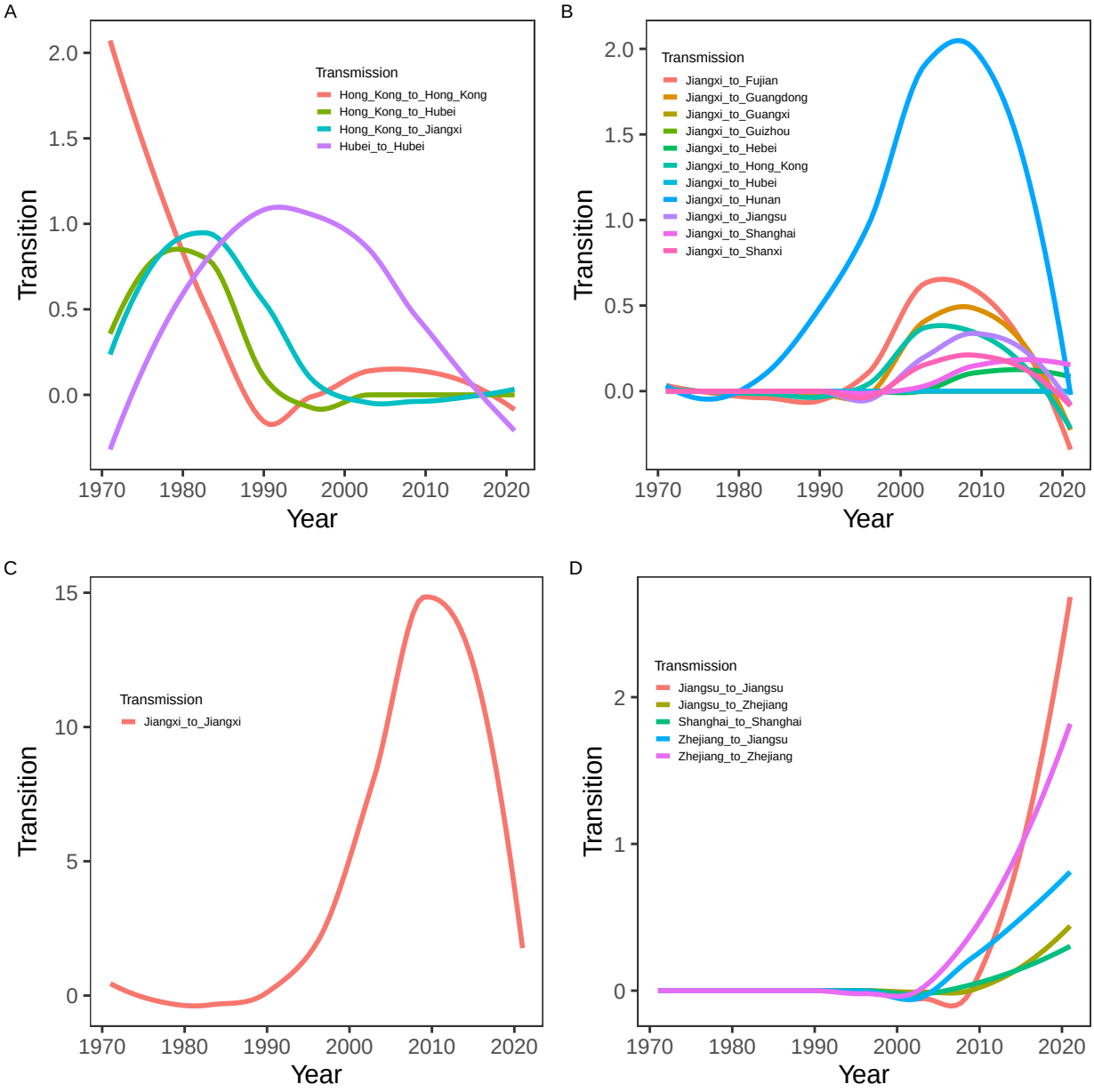
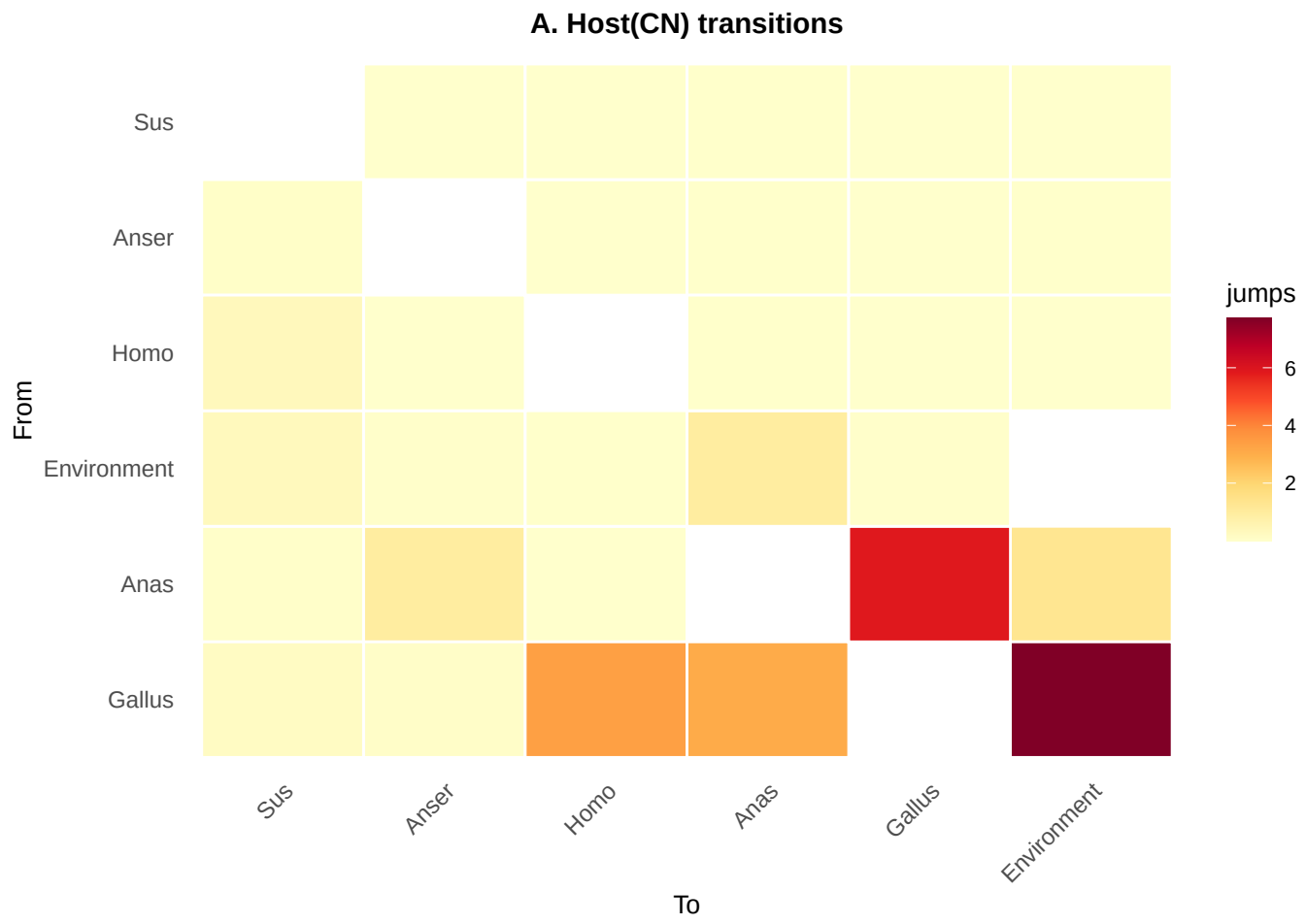
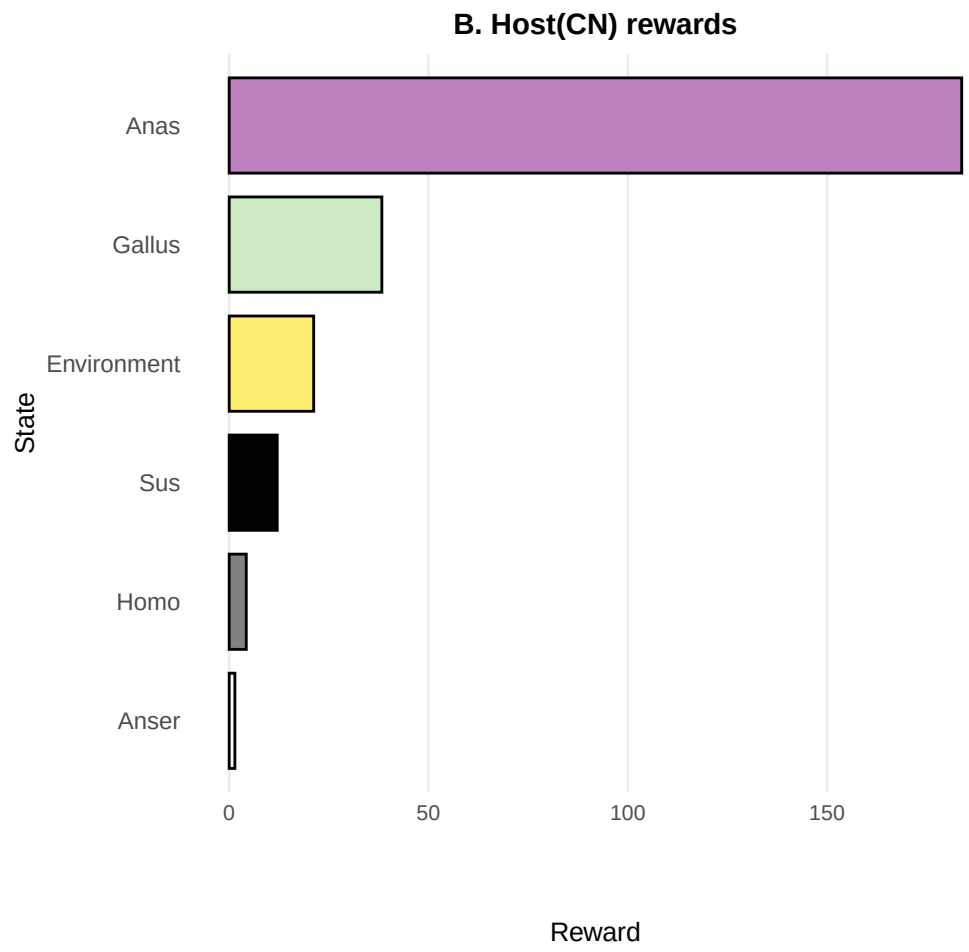
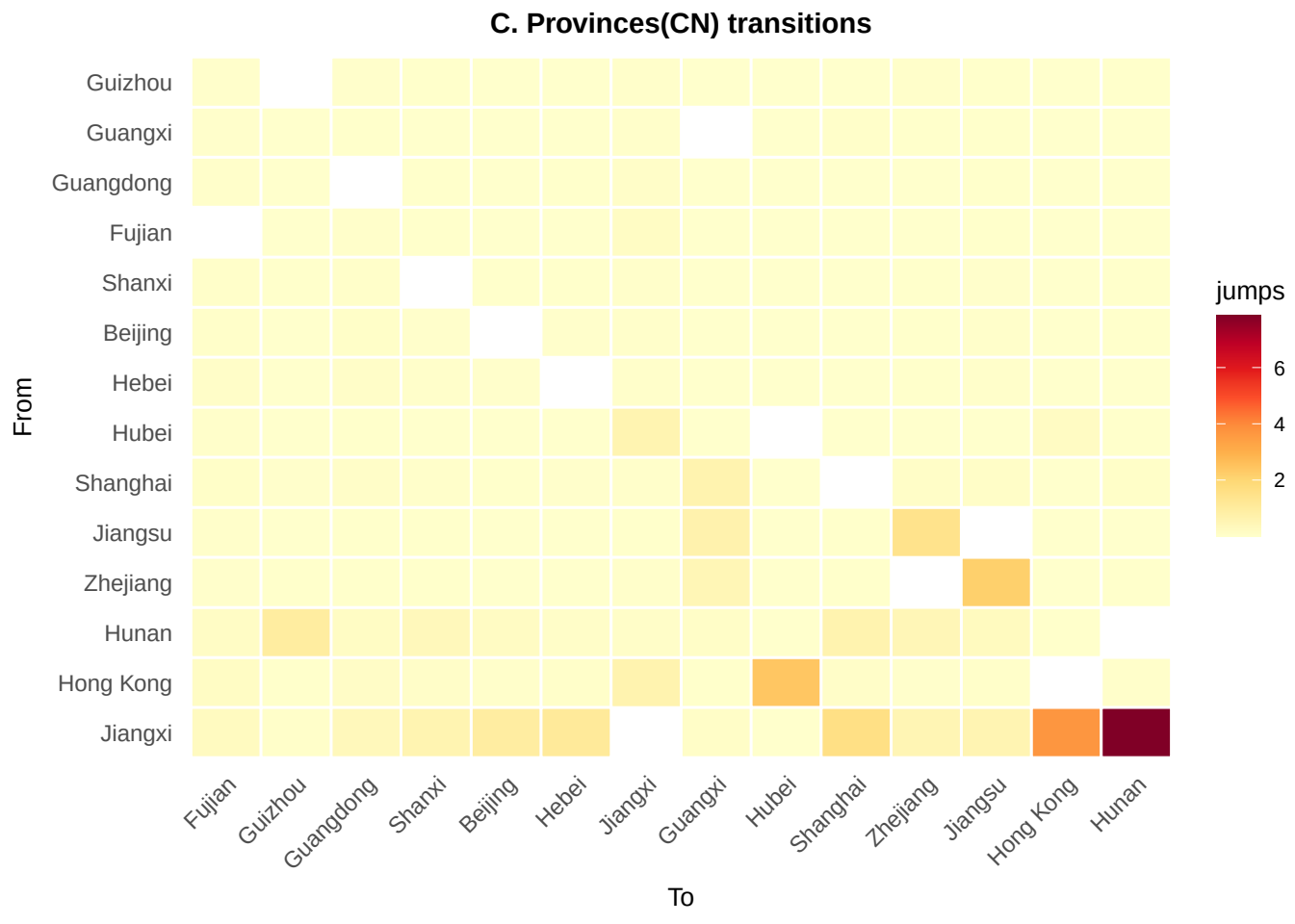


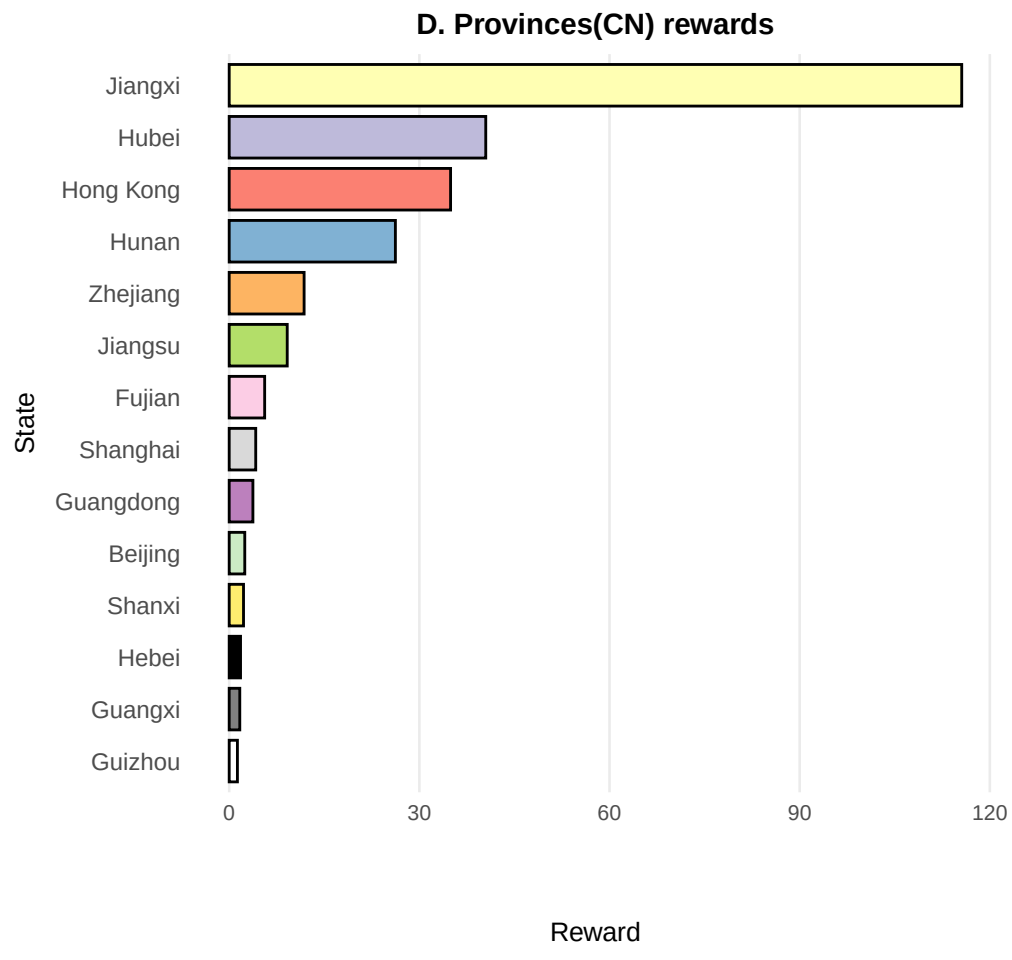
Image not available with this version

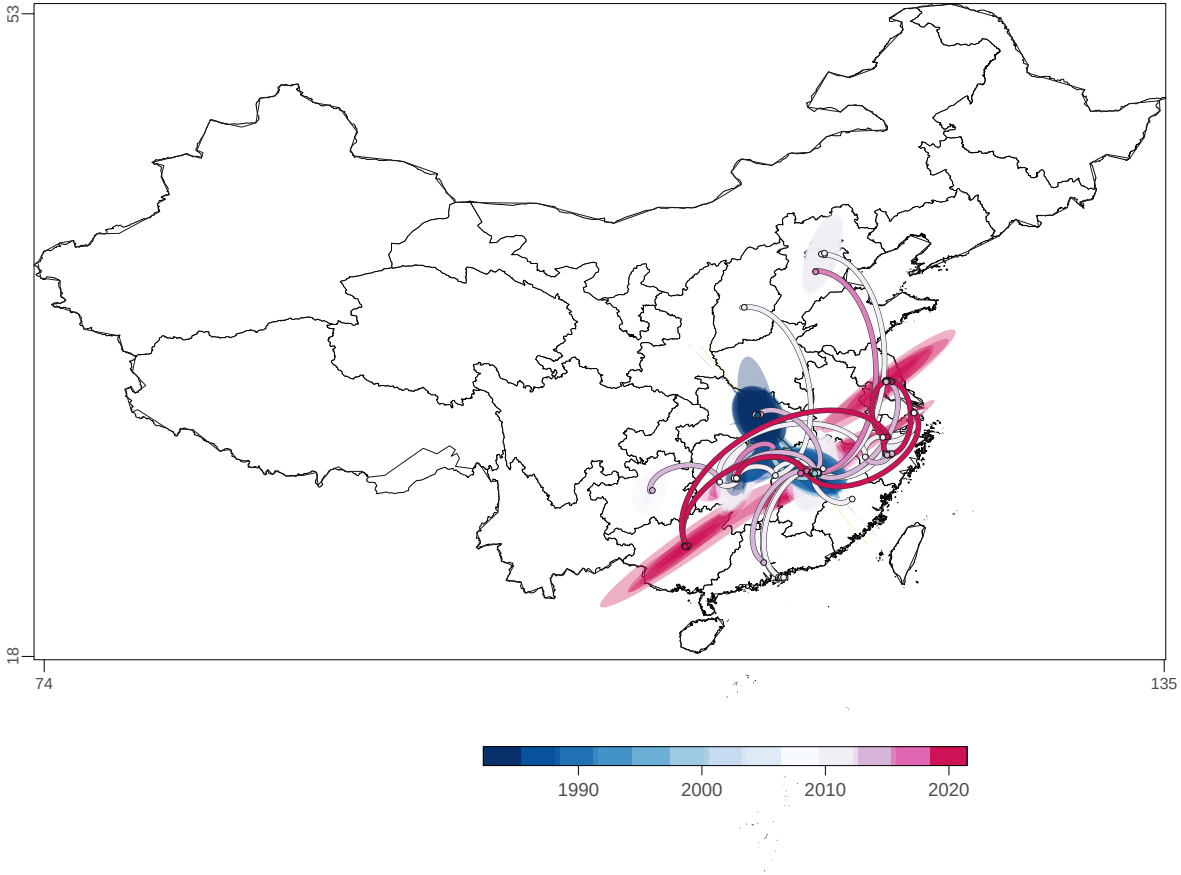

A
Transmission
Hong_Kong_to_Hong_Kong
Hong_Kong_to_Hubei
Hong_Kong_to_Jiangxi
Hubei_to_Hubei
Transition
Year
B
Transmission
Jiangxi_to_Fujian
Jiangxi_to_Guangdong
Jiangxi_to_Guangxi
Jiangxi_to_Guizhou
Jiangxi_to_Hebei
Jiangxi_to_Hong_Kong
Jiangxi_to_Hubei
Jiangxi_to_Hunan
Jiangxi_to_Jiangsu
Jiangxi_to_Shanghai
Jiangxi_to_Shanxi
Transition
Year
C
Transmission
Jiangxi_to_Jiangxi
Transition
Year
D
Transmission
Jiangsu_to_Jiangsu
Jiangsu_to_Zhejiang
Shanghai_to_Shanghai
Zhejiang_to_Jiangsu
Zhejiang_to_Zhejiang
Transition
Year

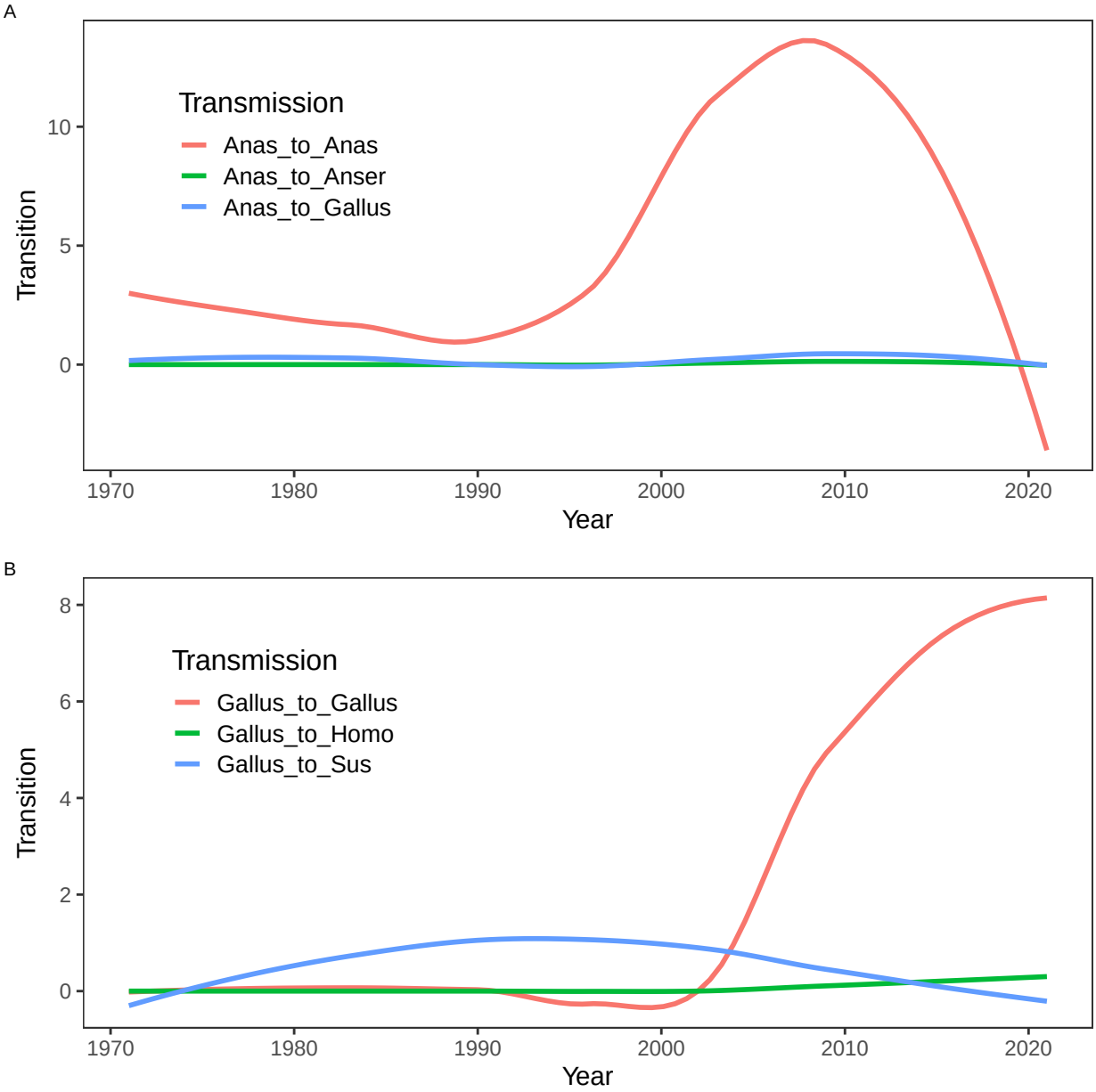

A. Host(CN) transitions
Sus
Anser
Homo
Environment
Anas
Gallus
From
Sus
Anser
Homo
Anas
Gallus
Environment
To
jumps
6
4
2

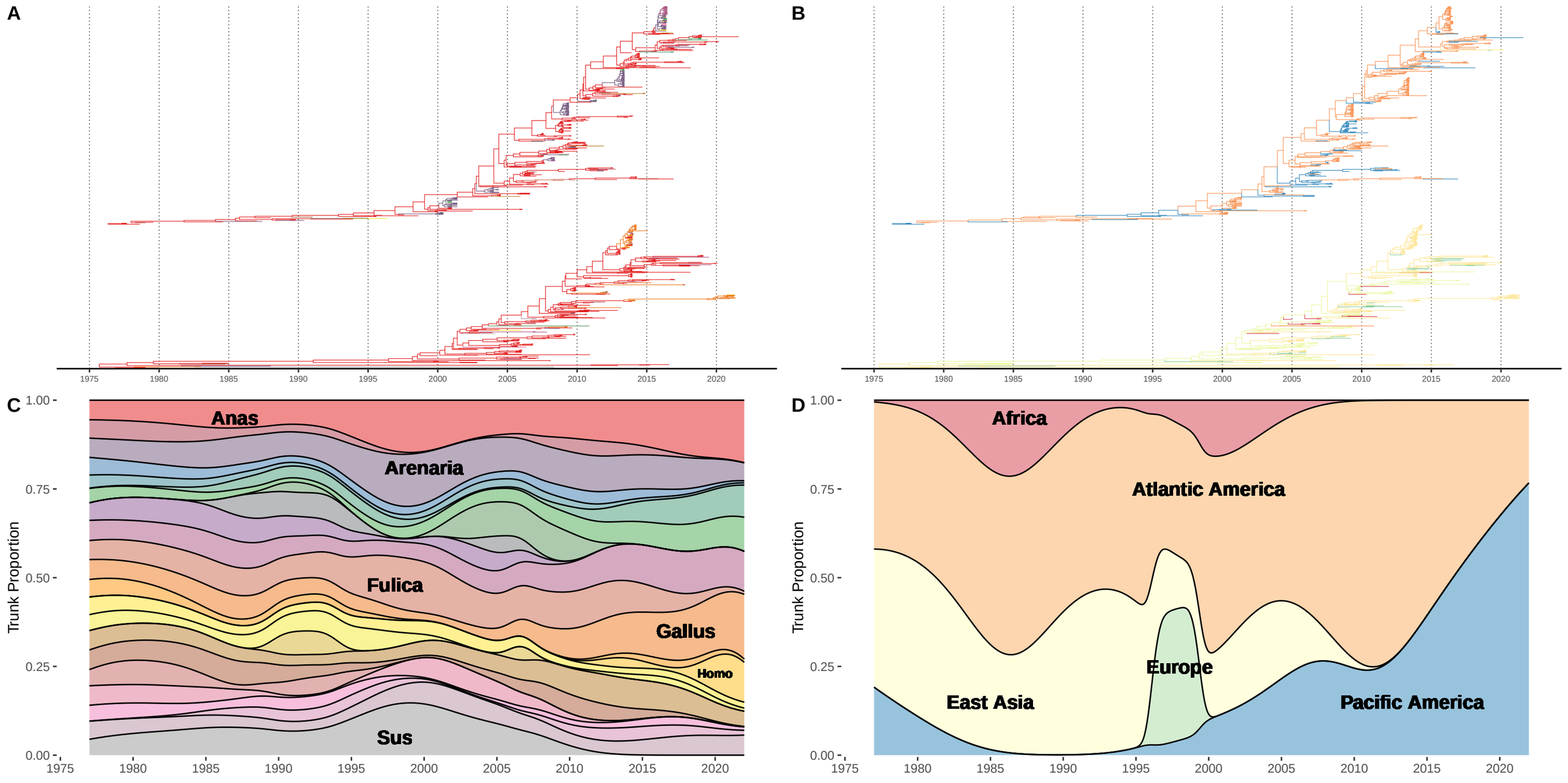

B. Host(CN) rewards
Anas
Gallus
Environment
Sus
Homo
Anser
State
0
50
100
150
Reward

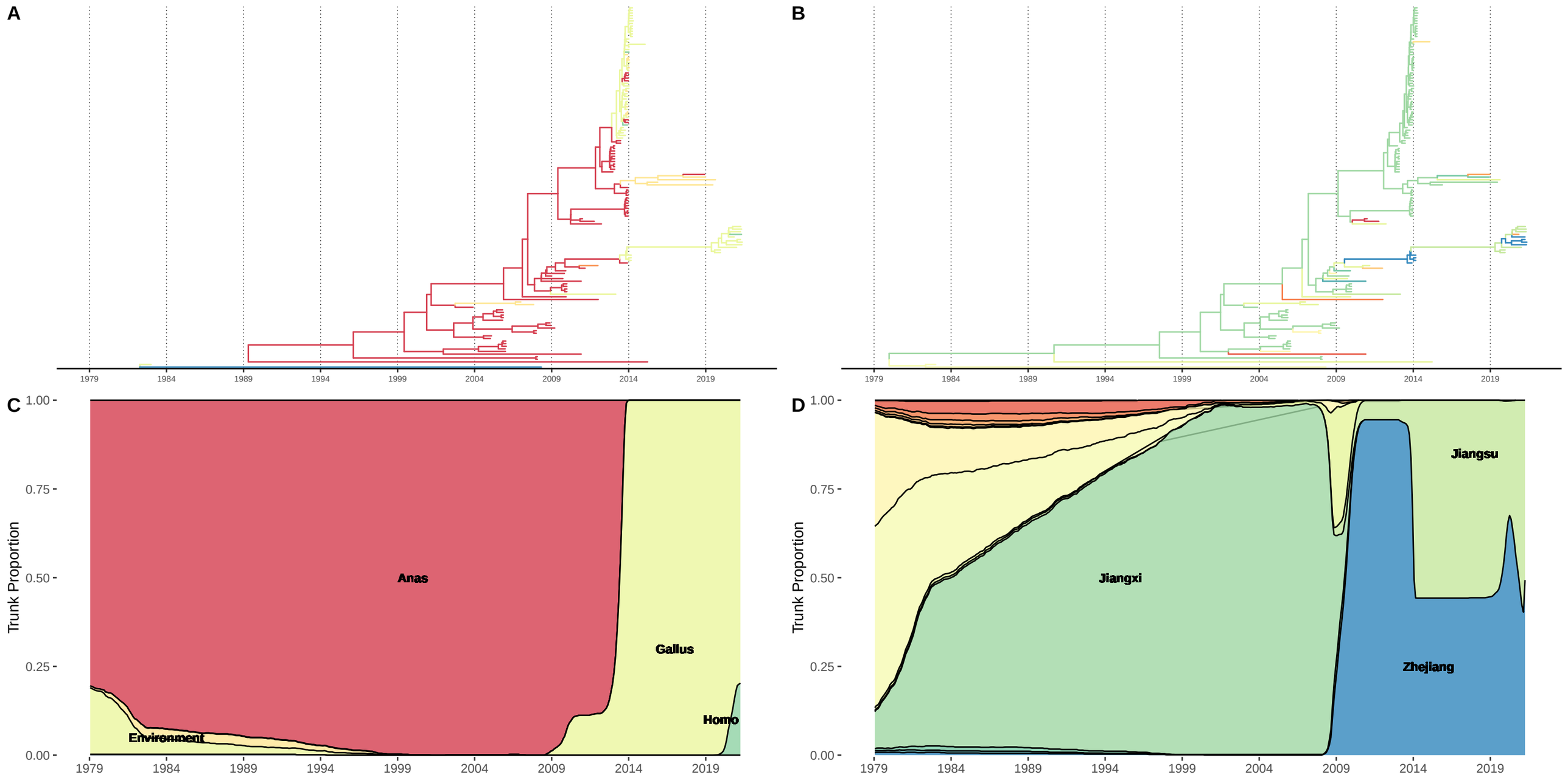

C. Provinces(CN) transitions
Guizhou
Guangxi
Guangdong
Fujian
Shanxi
Beijing
Hebei
Hubei
Shanghai
Jiangsu
Zhejiang
Hunan
Hong Kong
Jiangxi
From
Fujian
Guizhou
Guangdong
Shanxi
Beijing
Hebei
Jiangxi
Guangxi
Hubei
Shanghai
Zhejiang
Jiangsu
Hong Kong
Hunan
To
jumps
6
4
2

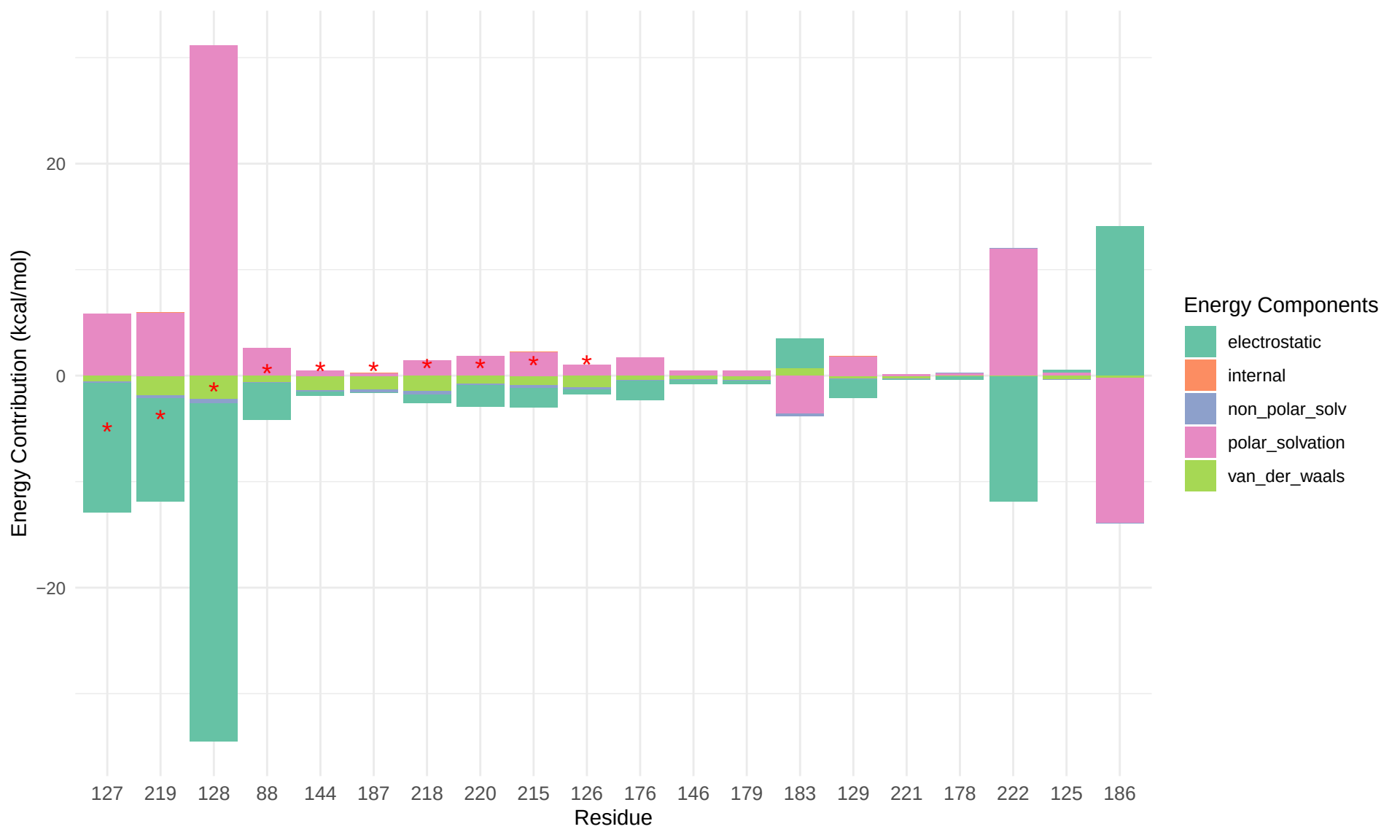

D. Provinces(CN) rewards
Jiangxi
Hubei
Hong Kong
Hunan
Zhejiang
Jiangsu
Fujian
Shanghai
Guangdong
Beijing
Shanxi
Hebei
Guangxi
Guizhou
State
0
30
60
90
120
Reward

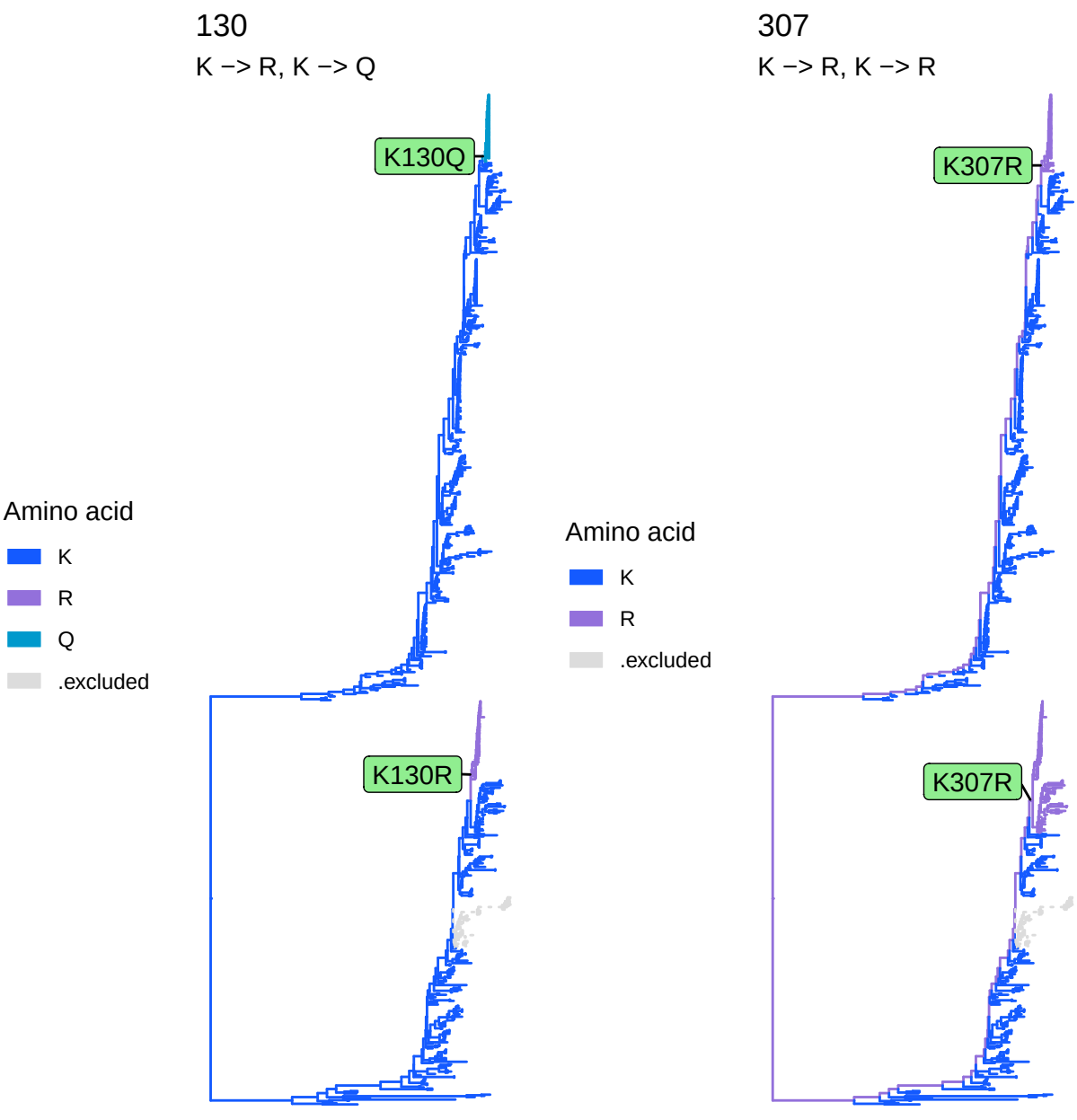

53
18
74
135
1990
2000
2010
2020


A
Transmission
Anas_to_Anas
Anas_to_Anser
Anas_to_Gallus
Transition
10
5
0
1970
1980
1990
2000
2010
2020
Year
B
Transmission
Gallus_to_Gallus
Gallus_to_Homo
Gallus_to_Sus
Transition
8
6
4
2
0
1970
1980
1990
2000
2010
2020
Year


A
B
1975
1980
1985
1990
1995
2000
2005
2010
2015
2020
C
Trunk Proportion
1.00
0.75
0.50
0.25
0.00
Anas
Arenaria
Fulica
Gallus
Homo
Sus
D
Africa
Atlantic America
Europe
East Asia
Pacific America


A
B
C
D
1979
1984
1989
1994
1999
2004
2009
2014
2019
1.00
0.75
0.50
0.25
0.00
Trunk Proportion
Anas
Gallus
Homo
Environment
Jiangsu
Jiangxi
Zhejiang


Energy Contribution (kcal/mol)
20
0
−20
127
219
128
88
144
187
218
220
215
126
176
146
179
183
129
221
178
222
125
186
Residue
Energy Components
electrostatic
internal
non_polar_solv
polar_solvation
van_der_waals


130
K –> R, K –> Q
K130Q
K130R
Amino acid
K
R
Q
.excluded
307
K –> R, K –> R
K307R
K307R
Amino acid
K
R
.excluded

Supplementary Files

This is a list of supplementary files associated with this preprint. Click to download.

- S03H10PopSize.pdf
- S02roottotipregression.pdf
- S5H10HAtreesub.pdf
- S01H10OrderSankey.pdf
- S4H10geoclustermap.pdf